(C) Expression of HLA-DR and other activation markers (CD11a, CD38, and CD150) by peripheral blood $CD4^+$ T cells. Representative flow cytometry profiles are shown from one of four hNOJ (IR+) mice at 16 wk post-transplantation. (D) Percentage of $HLA\text{-}DR^+$ cells in the naïve, CM, EM_{early}, and $EM_{int/late}$ subsets of peripheral blood $CD4^+$ T cells isolated from hNOJ mice at 16 wk post-transplantation ($n=4$; two hNOJ (IR+) and two hNOJ (IR−) mice) and from humans ($n=3$). Data are expressed as the mean ± SD. Significant differences ($^{**}P<0.01$, $^{***}P<0.001$) were determined by Tukey's multiple comparison test. (E) Association between the percentage of each $CD4^+$ T cell subset and that of $HLA\text{-}DR^+$ cells in the peripheral blood $CD4^+$ T cell population. Data were obtained from peripheral blood samples routinely collected from hNOJ (IR+) and hNOJ (IR−) mice within 28 wk post-transplantation (50 data points obtained from 25 mice (upper panels) and 59 data points obtained from 21 mice (lower panels), respectively). Spearman's rank correlation coefficient was used for statistical analysis.
doi:10.1371/journal.pone.0053495.g004

leukocytes within the total PBMC population) than hNOJ (IR−) mice ($n=13$) during the course of the experiment (Figure 2A).

Furthermore, we examined the effects of irradiation on the engraftment of HSCs in the BM of hNOJ mice in which $hCD45^+$ leucocytes were observed. hNOJ (IR+) mice showed a significantly higher percentage of $CD34^+$ cells within the total BM cell population (an average of 3.7%; $n=5$) than hNOJ (IR−) mice (an average of 0.3%; $n=6$) at 8 wk post-transplantation (Figure 2B). The percentage of $CD34^+$ cells within the total BM cell population was positively correlated with the percentage of $hCD45^+$ leukocytes within the total PBMC population at 8 wk post-transplantation ($R=0.9364$, $P<0.001$, $n=11$ [five hNOJ (IR+) and six hNOJ (IR−) mice]; Figure 2C). These results indicate that irradiation augments the chimerism of human hematopoietic cells due to the enhanced engraftment of HSCs in the BM of hNOJ mice.

Next, we investigated the development of hematopoietic cell subpopulations in hNOJ (IR+) and hNOJ (IR−) mice ($n=22$ and $n=13$, respectively). The reconstituted $hCD45^+$ leukocytes within the total PBMC populations from hNOJ (IR+) and hNOJ (IR−) mice comprised $CD19^+$ B cells, $CD14^+$ monocytes, and $CD3^+$ T cells (including $CD4^+$ and $CD8^+$ T cells); however, the development of each subpopulation was different (Figure 2D). $CD19^+$ B cells developed early in both hNOJ (IR+) and hNOJ (IR−) mice, as observed at 8 wk post-transplantation, before gradually declining over time (Figure 2D, left upper panel). $CD14^+$ monocytes also developed during the early phase post-transplantation in hNOJ (IR+) mice, but were rare in hNOJ (IR−) mice. In general, the percentage of all the subpopulations was significantly lower in hNOJ (IR−) mice than in hNOJ (IR+) mice up until 16 wk post-transplantation, although the percentage of $CD14^+$ monocytes in hNOJ (IR−) mice gradually increased with time (Fig. 2D, right upper panel). In apparent contrast to the earlier development of $CD19^+$ B cells, the development of $CD3^+$ T cells was delayed; they were clearly apparent at around 12 wk post-transplantation in both hNOJ (IR+) and hNOJ (IR−) mice (Figure 2D, left and right lower panels), consistent with previous reports of other conventional humanized mouse models [16,20,36,37]. The percentage of $CD3^+$ T cells reflected that of $CD4^+$ T cells; the level of $CD4^+$ T cells was higher than that of $CD8^+$ T cells, and their developmental level tended to be higher in hNOJ (IR+) mice than in hNOJ (IR−) mice, although no statistically significant differences were observed between hNOJ (IR+) and hNOJ (IR−) mice (Figure 2D, lower left and right panels). However, both the $CD4^+$ and $CD8^+$ T cell percentages within the total PBMC population in hNOJ (IR+) mice were significantly higher than those in hNOJ (IR−) mice at almost time-points up until 16 wk post-transplantation (Figure 2E, lower left and right panels). It is noteworthy that reconstitution of $CD4^+$ T cells was detected in more hNOJ (IR+) mice (18 of 22 mice) than hNOJ (IR−) mice (4 of 13 mice) at 8 wk post-transplantation, although the averaged percentages were slightly lower (0.12±0.33% and 0.02±0.03% $CD4^+$ T cells, respectively, within the total PBMC population). The percentages of other human hematopoietic cells within the total PBMC population, such as $CD19^+$ B cells, $CD14^+$ monocytes and $CD8^+$ T cells, were also higher in hNOJ (IR+) mice than in hNOJ (IR−) mice at all time-points up to 16 wk post-transplantation (Figure 2E). Taken together, these results indicate that irradiation contributes to the greater reconstitution of human hematopoietic cells in these humanized mice.

Differentiation of $CD4^+$ T Cells in hNOJ Mice

A reliable differentiation pathway for human $CD4^+$ T cells has been proposed: an antigen-experienced naïve subset differentiates into a central memory (CM) subset, followed by differentiation into an effector memory (EM) subset, before finally differentiating into a terminal effector subset [38,39]. To investigate the differentiation stage of $CD4^+$ T cells reconstituted in hNOJ mice, we used hNOJ (IR+) and hNOJ (IR−) mice in which $CD4^+$ T cells had developed by 12 wk post-transplantation.

As shown in Figure 3A, we divided $CD4^+$ T cells into four subsets based on their expression of cell surface antigens as previously reported: naïve ($CD45RA^+CCR7^+CD27^+$), CM ($CD45RA^-CCR7^+CD27^+$), EM_{early} ($CD45RA^-CCR7^-CD27^+$) and $EM_{int/late}$ ($CD45RA^-CCR7^-CD27^-$) [38,40,41]. Flow cytometric analysis using PBMCs routinely collected from hNOJ (IR+) and hNOJ (IR−) mice ($n=18$ and $n=6$, respectively) demonstrated that the percentage of each $CD4^+$ T cell subset showed similar changes in hNOJ (IR+) and hNOJ (IR−) mice by 16 wk post-transplantation (Figure 3B). The naïve subset was dominant at 12 wk post-transplantation; however, the percentage decreased markedly, reaching a steady level of approximately 20% at 20 wk post-transplantation in hNOJ (IR−) mice. In sharp contrast with the changes over time observed for the naïve subset, the percentages of the EM_{early} and $EM_{int/late}$ subsets in hNOJ (IR−) mice gradually increased over time. The percentage of the CM subset in hNOJ (IR−) mice remained unchanged at 10−20% throughout the course of the experiment. The percentage of each subset in the hNOJ mice during the early phase (12 wk) post-transplantation was almost identical to that in human PBMCs, in which the naïve subset was also dominant (approximately 50%, $n=10$) (Figure 3C).

Activation Status of $CD4^+$ T Cells in hNOJ Mice

The activation status of the reconstituted $CD4^+$ T cells was assessed by flow cytometric analysis of PBMCs isolated from hNOJ (IR+) and hNOJ (IR−) mice ($n=18$ and $n=6$, respectively), based on their expression of early and late activation markers (CD69 and HLA-DR, respectively). We found that the percentage of $CD69^+CD4^+$ T cells increased in hNOJ (IR+) mice at 16 wk post-transplantation compared with that observed at 12 wk post-transplantation ($P=0.0007$). In hNOJ (IR−) mice, the percentage of $CD69^+CD4^+$ T cells appeared to show a transient increase at 16 wk post-transplantation; however, no significant differences were observed between 16 wk post-transplantation and the other time-points (Figure 4A, upper panel). By contrast, the percentage of $HLA\text{-}DR^+CD4^+$ T cells increased in both hNOJ (IR+) and hNOJ (IR−) mice at 16 wk post-transplantation compared with

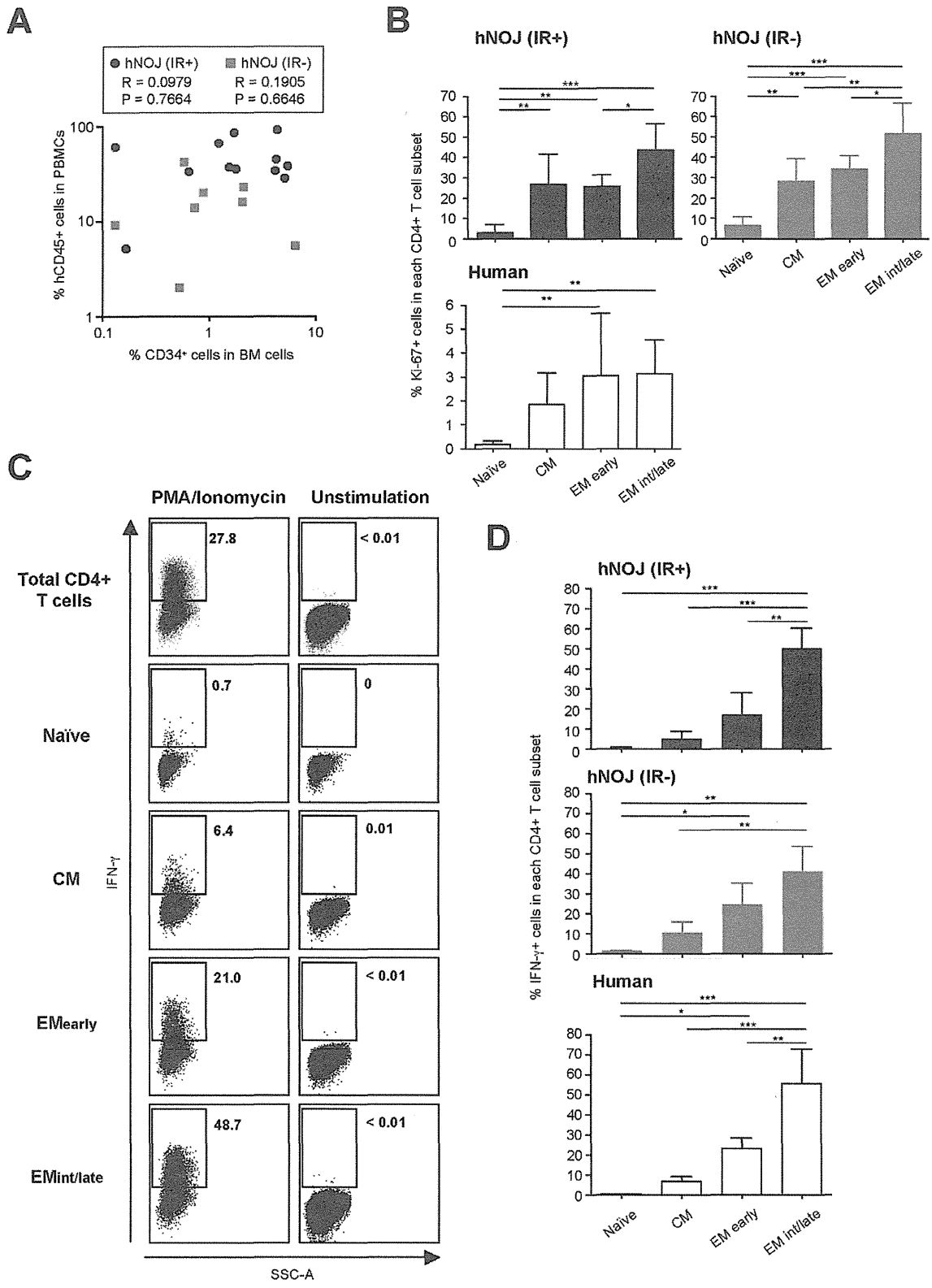

Figure 5. Possible occurrence of HSP of CD4$^+$ T Cells in hNOJ mice. (A) Association between the percentage of hCD45$^+$ cells within the PBMC population and that of CD34$^+$ cells in the BM cells from hNOJ (IR+) and hNOJ (IR−) mice at ≥16 wk post-transplantation ($n=12$ and $n=8$, respectively). Spearman's rank correlation coefficient was used for statistical analysis. (B) Percentage of Ki-67$^+$ cells among naïve, CM, EM_{early}, and $EM_{int/late}$ subsets of splenic CD4$^+$ T cells from hNOJ (IR+) and hNOJ (IR−) mice at ≥16 wk post-transplantation ($n=6$ and $n=6$, respectively) and from human PBMCs ($n=10$). Data are expressed as the mean ± SD. Significant differences ($^*P<0.05$, $^{**}P<0.01$, $^{***}P<0.001$) were determined by Tukey's

multiple comparison test. (C and D) *Ex vivo* IFN-γ production by $CD4^+$ T cells after stimulation with PMA/ionomycin. $CD4^+$ T cells were prepared from the spleens of hNOJ (IR+) and hNOJ (IR−) mice at ≥16 wk post-transplantation or from human PBMCs. (C) Representative flow cytometry profiles showing the proportion of IFN-γ^+ cells within each of the $CD4^+$ T cell subsets from a hNOJ (IR+) mouse at 16 wk post-transplantation. (D) Cumulative data showing the percentage of IFN-γ^+ cells within each of the $CD4^+$ T cell subsets from hNOJ (IR+) and hNOJ (IR−) mice and humans ($n=3$, $n=3$, and $n=4$, respectively). Data are expressed as the mean ± SD. Significant differences ($^*P<0.05$, $^{**}P<0.01$, $^{***}P<0.001$) were determined by Tukey's multiple comparison test.
doi:10.1371/journal.pone.0053495.g005

12 wk post-transplantation, and the difference was statistically significant ($P<0.0001$ and $P<0.0313$). Also, this increase was maintained at about 50−60% beyond 16 wk post-transplantation in hNOJ (IR−) mice (Figure 4A, lower panel). To assess the activation status of $CD4^+$ T cells in other organs, such as the spleen and BM, we next performed an experiment using hNOJ (IR+) mice at 8 wk post-transplantation and hNOJ (IR−) mice at ≥20 wk post-transplantation as representative examples of early- and late-phase, respectively, $CD4^+$ T cell development. We found that the expression of HLA-DR by peripheral blood $CD4^+$ T cells isolated from hNOJ mice was consistent with that by cells isolated from the spleen and BM: lower expression of HLA-DR (7.7% and 17.1% in two hNOJ (IR+) mice) during the early phase (8 wk) post-transplantation, which is also equivalent to that in human PBMCs, and higher expression (68.7−93.8% in four hNOJ (IR−) mice) during the later phase (≥20 wk) post-transplantation (Figure 4B). To address whether HLA-DR expression actually reflects the activation status of reconstituted $CD4^+$ T cells, we examined the expression of other activation markers: CD11a, CD38, and CD150. Figure 4C shows representative flow cytometry profiles obtained using peripheral blood $CD4^+$ T cells isolated from one of four hNOJ (IR+) mice at 16 wk post-transplantation. HLA-DR^+CD4^+ T cells also expressed these markers, confirming the highly activated status of the HLA-DR^+CD4^+ T cells reconstituted in hNOJ mice.

We further investigated whether the activation status of $CD4^+$ T cells was associated with their differentiation stage. When the total percentage of HLA-DR^+ cells within the peripheral blood $CD4^+$ T cell subset populations was examined, we found that the memory $CD4^+$ T cell subsets, particularly the $EM_{int/late}$ subset, made up a significantly higher proportion of this percentage than the naïve subset ($n=4$; two hNOJ (IR+) and two hNOJ (IR−) mice; Figure 4D). The different HLA-DR expression patterns between the $CD4^+$ T cell subsets were similar in human PBMCs ($n=3$), although the expression levels were much lower than those in hNOJ mice (Figure 4D). To further address this differentiation stage-dependent level of HLA-DR expression by $CD4^+$ T cells, we compared the percentage of each $CD4^+$ T cell subset with the percentage of HLA-DR^+ cells within the total $CD4^+$ T cell population using data obtained from peripheral blood samples routinely collected from hNOJ (IR+) and hNOJ (IR−) mice ($n=25$ and $n=21$, respectively) within 25 wk and 28 wk post-transplantation, respectively. We found that the percentage of HLA-DR^+ cells positively correlated with that of the EM_{early} and $EM_{int/late}$ subsets, and inversely correlated with that of the naïve subset, in both hNOJ (IR+) and hNOJ (IR−) mice (Figure 4E). However, there was no significant correlation between the percentage of HLA-DR^+ cells and that of the CM subset in either hNOJ (IR+) or hNOJ (IR−) mice, indicating an intermediate stage at which cells are acquiring the activation phenotype (Figure 4E). Taken together, reconstituted $CD4^+$ T cells in hNOJ mice express a unique phenotype compared with human peripheral blood $CD4^+$ T cells: activated EM subsets predominate with time after transplantation.

Homeostatic Peripheral Expansion of $CD4^+$ T Cells May Occur in hNOJ Mice

When the percentage of $hCD45^+$ leukocytes within the total PBMC population was compared with that of $CD34^+$ cells within the total BM cell population during the later phase (≥16 wk) post-transplantation, no significant correlation was observed in either hNOJ (IR+) or hNOJ (IR−) mice ($n=12$ and $n=8$, respectively) (Figure 5A). These results prompted us to assume that $CD4^+$ T cell proliferation/expansion was predominant in hNOJ mice during the late phase post-transplantation. Therefore, we next examined the expression of a proliferation marker, Ki-67, by reconstituted $CD4^+$ T cells using flow cytometry to assess the proliferative capacity at different differentiation stages. $CD4^+$ T cells were prepared from the spleens of hNOJ (IR+) and hNOJ (IR−) mice during the later phase (≥16 wk) post-transplantation ($n=6$ and $n=6$, respectively). $CD4^+$ T cells isolated from human PBMCs ($n=10$) were used as a control. The results showed that Ki-67^+ cells were present within the memory $CD4^+$ T cell subsets (CM, EM_{early} and $EM_{int/late}$) at higher percentages than within the naïve subset (Figure 5B, upper two panels). A higher percentage of Ki-67^+ cells was also observed in the memory subsets within the human PBMC population than in the naïve subset; however, the levels were much lower than those observed in the hNOJ mice (Figure 5B, lower panel). These results support the notion that increased $CD4^+$ T cell proliferation/expansion occurs in hNOJ mice during the later phase post-transplantation.

HSP of $CD4^+$ T cells involves both slow and rapid proliferation pathways. The slow pathway is IL-7-dependent and results in limited cell activation and differentiation, whereas the latter is T cell receptor (TCR)-dependent and IL-7-independent and results in robust cell activation and differentiation into a memory phenotype with the capacity to produce IFN-γ [25,26]. The term "HSP" is generally used to indicate the former; the latter is often referred to as "spontaneous HSP" [25] or "homeostatic peripheral expansion (HPE)" [26]. It was assumed that HPE-type HSP might occur in hNOJ mice, as described elsewhere [27,28]; therefore, we examined the IFN-γ-producing capacity of $CD4^+$ T cells isolated from the spleens of hNOJ (IR+) and hNOJ (IR−) mice ($n=3$ and $n=3$, respectively) during the later phase (16 and 26 wk, respectively) post-transplantation by stimulating them with or without PMA plus ionomycin. Flow cytometric analysis of intracellular IFN-γ staining showed substantial numbers of IFN-γ-producing cells within the $EM_{int/late}$ subset after PMA/ionomycin stimulation; the data were similar when $CD4^+$ T cells from human PBMCs were used in the experiment ($n=4$) (Figure 5C and 5D). No IFN-γ-producing cells were detectable in any of the $CD4^+$ T cell subsets from hNOJ (IR+) and hNOJ (IR−) mice, or in human PBMCs without PMA/ionomycin stimulation (Figure 5C and data not shown).

Next, we measured the concentrations of cytokines (IL-2, IL-7, and IL-15, all of which are involved in $CD4^+$ T cell proliferation [24,42]), in plasma prepared from peripheral blood samples taken from hNOJ (IR+) and hNOJ (IR−) mice ($n=9$ and $n=13$, respectively) at 12, 16, and (occasionally) 20 wk post-transplantation. However, none of these cytokines were present at detectable levels (limit of detection = <3.2 pg/ml).

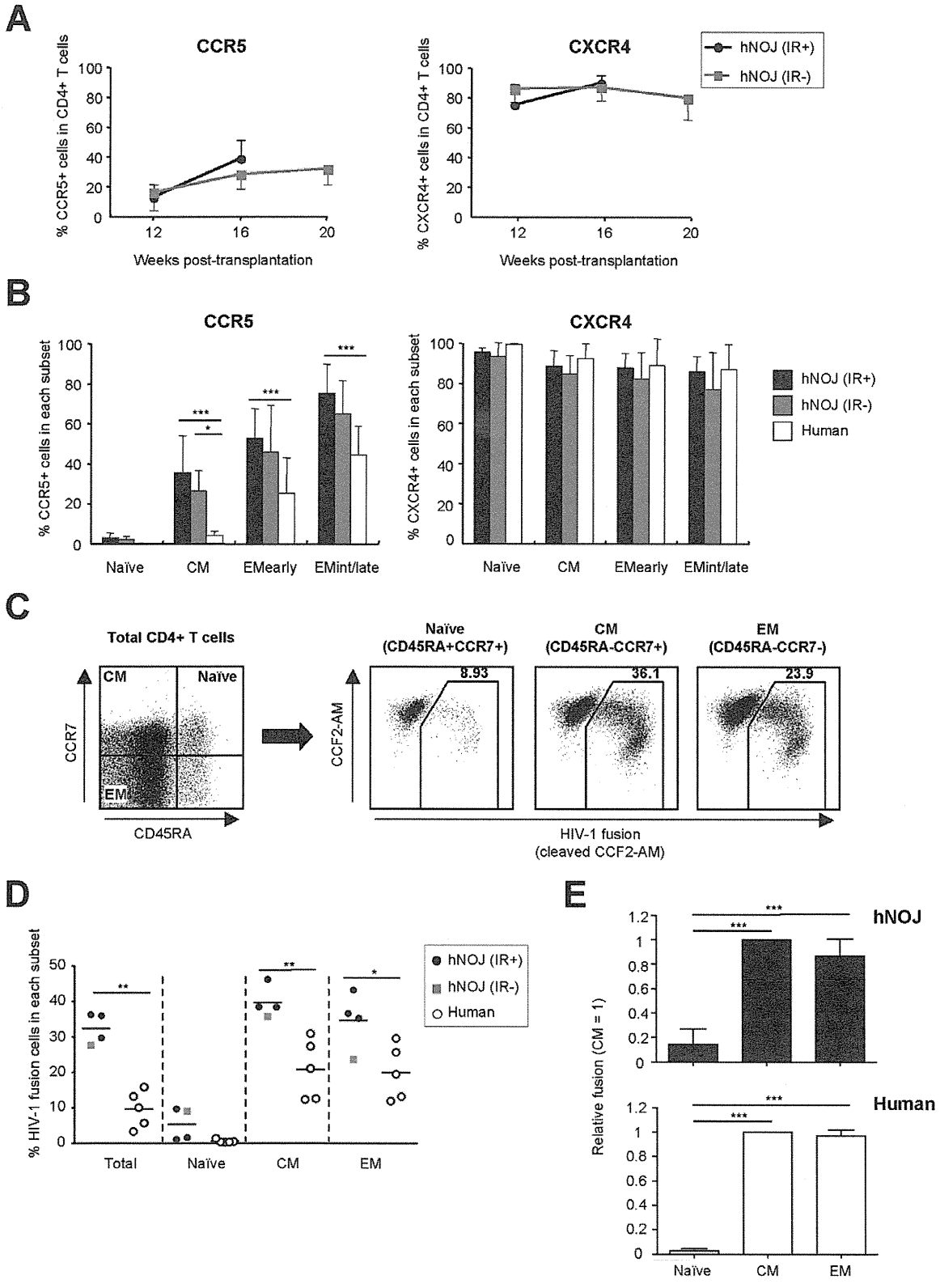

Figure 6. HIV-1 co-receptors, CCR5 and CXCR4, expression profiles and *ex vivo* R5 HIV-1 infectivity of CD4$^+$ T Cells in hNOJ mice. (A) Changes in the percentage of CCR5$^+$ (left) and CXCR4$^+$ (right) cells within the peripheral blood CD4$^+$ T cell population isolated from hNOJ (IR+) and hNOJ (IR−) mice ($n=18$ and $n=6$, respectively). Data are expressed as the mean ± SD. (B) Percentage of CCR5$^+$ and CXCR4$^+$ cells within the naïve, CM, EM_{early}, and $EM_{int/late}$ subsets of peripheral blood CD4$^+$ T cells isolated from hNOJ mice at 16 wk post-transplantation ($n=18$ and $n=6$, respectively) and from humans ($n=5$). Data are expressed as the mean ± SD. Significant differences ($^*P<0.05$, $^{***}P<0.001$) were determined by two-

way factorial ANOVA with the Bonferroni multiple comparison test. (C, D, E) Fusion assay using R5 HIV-1 and $CD4^+$ T cells. Splenic $CD4^+$ T cells from hNOJ mice at ≥17 wk post-transplantation ($n=4$; three hNOJ (IR+) mice and one hNOJ (IR−) mouse) or peripheral blood $CD4^+$ T cells from humans ($n=5$) were infected *ex vivo* with HIV-$1_{NL\text{-}AD8\text{-}D\text{-}BlaM\text{-}Vpr}$. (C) Naïve, CM, and EM subsets of $CD4^+$ T cells (gated on $CD3^+CD4^+CD8^-$) were defined as $CD45RA^+CCR7^+$, $CD45RA^-CCR7^+$, and $CD45RA^-CCR7^-$, respectively, by flow cytometry. (D) Percentage of R5 HIV-1 fusion cells within the total $CD4^+$ T cell population and within the naïve, CM, and EM subsets in hNOJ mice and humans. Individual data points are plotted. The black lines represent the mean. Significant differences ($^*P<0.05$, $^{**}P<0.01$) were determined by the unpaired *t* test. (E) Relative ratio of R5 HIV-1 fusion among the naïve, CM, and EM subsets from hNOJ mice and humans. The level of R5 HIV-1 fusion in each of the $CD4^+$ T cell subsets relative to that in the corresponding CM subset. Data are expressed as the mean ± SD. Significant differences ($^{***}P<0.001$) were determined by Tukey's multiple comparison test.
doi:10.1371/journal.pone.0053495.g006

Taken together, these results support the notion that the time-dependent appearance of the activated memory $CD4^+$ T cell subset in hNOJ mice is due to HPE-type HSP.

Expression Profiles of CCR5 and CXCR4 in $CD4^+$ T Cells in hNOJ Mice

The expression profiles of the HIV-1 co-receptors, CCR5 and CXCR4, on $CD4^+$ T cells within the PBMC populations in hNOJ mice and humans were compared by flow cytometry. The percentage of $CCR5^+CD4^+$ T cells gradually increased over time in both hNOJ (IR+) and hNOJ (IR−) mice ($n=18$ and $n=6$, respectively) (Figure 6A, left panel). Consistent with this, a substantial percentage of $CCR5^+$ cells was observed in both hNOJ (IR+) and hNOJ (IR−) mice ($n=18$ and $n=6$, respectively) and humans ($n=5$), depending on the differentiation status of the $CD4^+$ T cells (Figure 6B, left panel). However, clear differences between hNOJ mice and humans were observed. For example, more $CCR5^+$ cells were present within the $CD4^+$ T cell population in hNOJ mice than in humans, and the CM subset in hNOJ mice comprised 30−40% $CCR5^+$ cells, whereas in humans it comprised significantly fewer $CCR5^+$ cells (Figure 6B, left panel). In contrast to CCR5, CXCR4 expression was consistently observed on approximately 80% of $CD4^+$ T cells in both hNOJ (IR+) and hNOJ (IR−) mice ($n=18$ and $n=6$, respectively) throughout the course of the experiment (Figure 6A, right panel), although the percentage of CXCR4-expressing cells at an advanced differentiation stage tended to be slightly lower in both hNOJ (IR+) and hNOJ (IR−) mice ($n=18$ and $n=6$, respectively) (Figure 6B, right panel).

Ex vivo R5 HIV-1 Infectivity of Reconstituted $CD4^+$ T Cells

We next performed *ex vivo* experiments based on fusion assays using reconstituted $CD4^+$ T cells to examine the susceptibility to R5 HIV-1 infection. $CD4^+$ T cells were prepared from the spleens of hNOJ mice during the later phase (≥17 wk) post-transplantation ($n=4$; one hNOJ (IR+) and three hNOJ (IR−) mice) or from human PBMCs ($n=5$), and infected with R5 HIV-1 containing a Vpr/β-lactamase fusion protein (HIV-$1_{NL\text{-}AD8\text{-}D\text{-}BlaM\text{-}Vpr}$). Because of the limited number of detector channels on the flow cytometer, each $CD4^+$ T cell subset was defined as naïve ($CD45RA^+CCR7^+$), CM ($CD45RA^-CCR7^+$), or EM ($CD45RA^-CCR7^-$) in this experiment, and R5 HIV-1 fusion cells were detected within each subset (Figure 6C). In parallel with the low percentage of CCR5 expression, R5 HIV-1 fusion was rarely observed in the naïve subsets from both hNOJ mice and humans, confirming the CCR5-dependent infection of reconstituted $CD4^+$ T cells by R5 HIV-1.

As shown in Figure 6D, the CM and EM subsets from hNOJ mice contained significantly more R5 HIV-1 fusion cells than those derived from humans. When the amount of R5 HIV-1 fusion within each $CD4^+$ T cell subset was expressed as a value relative to that of the corresponding CM subset (which was set at 1), we found that the CM and EM subsets in both hNOJ mice and humans were highly susceptible to R5 HIV-1 compared with the naïve subset, indicating that the susceptibility to R5 HIV-1 among the $CD4^+$ T cell subsets was similar in hNOJ mice and humans (Figure 6E). Notably, despite the finding that the percentage of CCR5-expressing cells in the CM subset was nearly half that in the EM subsets (Figure 6B, left panel), R5 HIV-1 fused efficiently to both the CM and EM subsets (Figure 6D and 6E). This result is not surprising, as similar observations were also made in a simian immunodeficiency virus infection model [43]. Furthermore, the $CCR5^-$ CM subset expresses CCR5 mRNA and is very susceptible to R5 virus [44].

In vivo R5 HIV-1 Infection in hNOJ Mice

To investigate whether the different constitution of $CD4^+$ T cell subsets, i.e., naïve- or memory subset-rich, affected HIV-1 infectivity *in vivo*, we used hNOJ (IR+) mice at 10 wk post-transplantation ($n=7$) as the naïve-rich group and hNOJ (IR−) mice at ≥12 wk post-transplantation ($n=8$) as the memory-rich group. After the hNOJ mice were challenged intravenously with R5 HIV-1 (HIV-$1_{NL\text{-}AD8\text{-}D}$), the plasma viral load was monitored weekly by quantitative real-time RT-PCR up until 5 wk post-challenge.

Viral RNA was detected in the plasma of all naïve-rich hNOJ (IR+) mice at 1 wk post-challenge, and was maintained at around 1×10^5 copies/ml over time (Figure 7A, left panel). On the other hand, memory-rich hNOJ (IR−) mice showed a blunted plasma viral load during the early phase post-challenge; however, the viral load reached peak values that were approximately 1-log higher than those in naïve-rich hNOJ (IR+) mice by 5 wk post-challenge (Figure 7A, right panel). Of note, the viral load was undetectable in the plasma of two (G122-2 and G122-5) of the eight memory-rich hNOJ (IR−) mice by 1 and 2 wk post-challenge, respectively, and the mean value for the plasma viral load at 1 wk post-challenge in memory-rich hNOJ (IR−) mice was significantly lower than that in naïve-rich hNOJ (IR+) mice (Figure 7B). Surprisingly, when we compared the absolute number of peripheral blood $CD4^+$ T cells between naïve-rich hNOJ (IR+) and memory-rich hNOJ (IR−) mice just before challenge, we found that memory-rich hNOJ (IR−) mice had significantly more $CD4^+$ T cells (apart from for the naïve subset) than naïve-rich hNOJ (IR+) mice (Figure 7C), indicating that the absolute number of peripheral blood $CD4^+$ T cells at pre-challenge is not associated with the timing and level of the initial plasma viral load. However, the $CD4^+$ T cell constitution in memory-rich hNOJ (IR−) mice may contribute to subsequent virus replication, because the peak value for the plasma viral load during 5 wk post-challenge was significantly higher in memory-rich hNOJ (IR−) mice than in naïve-rich hNOJ (IR+) mice ($n=6$ and $n=7$, respectively; one hNOJ (IR+) and one hNOJ (IR−) mice were excluded from this analysis as the experiment was interrupted before 5 wk post-challenge) (Figure 7D).

To characterize the HIV-1-infected $CD4^+$ T cells further, three additional hNOJ (IR−) mice were analyzed at 2 wk post-challenge with R5 HIV-1 (Figure 8). HIV-1 infected cells were detected according to their expression of the fluorescent reporter, DsRed, by flow cytometry as described previously [29,45], and $CD4^+$ T

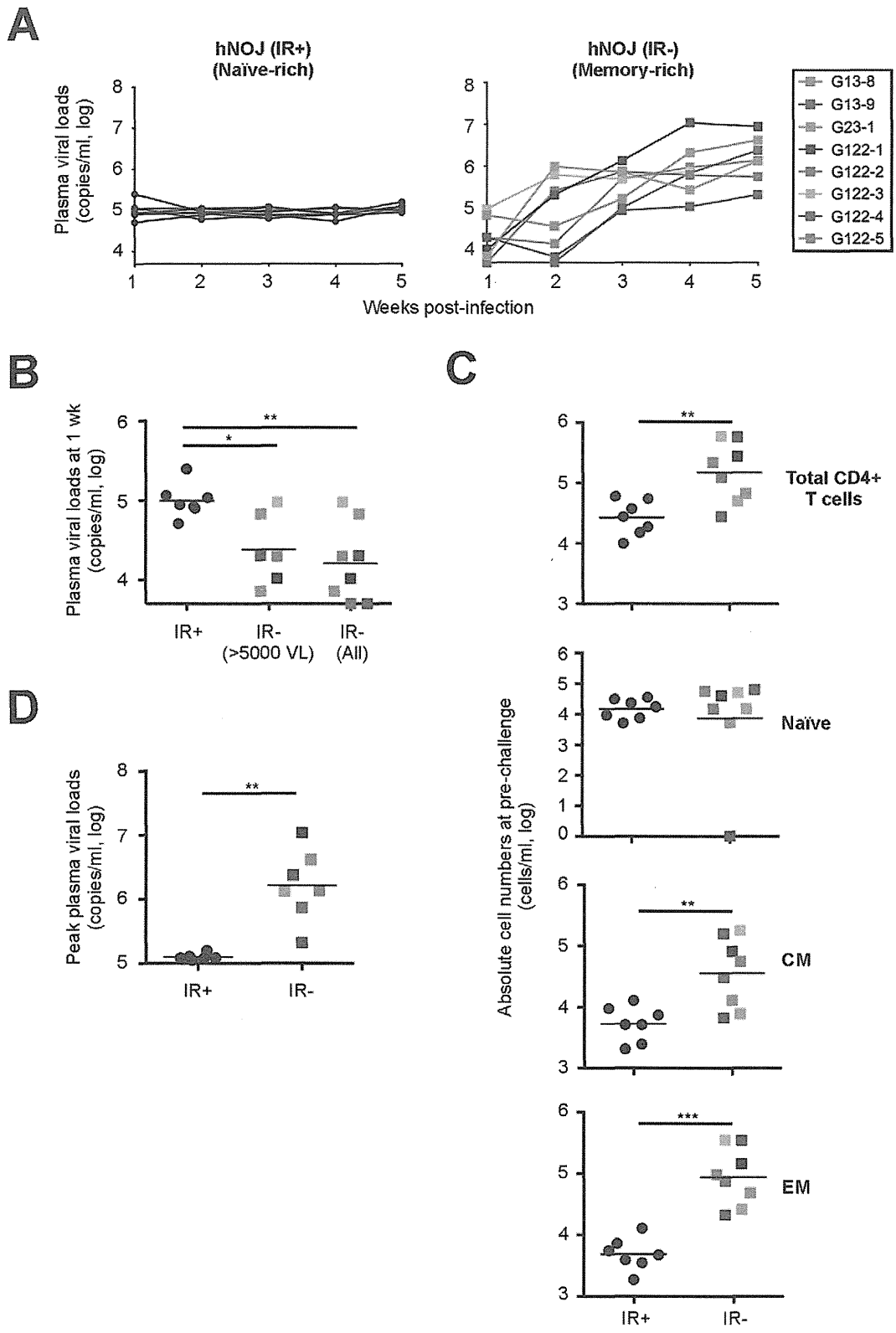

Figure 7. ***In vivo*** **R5 HIV-1 infection in hNOJ mice.** hNOJ mice were challenged intravenously with HIV-$1_{NL\text{-}AD8\text{-}D}$ and divided into two groups: naïve-rich hNOJ (IR+) mice at 10 wk post-transplantation ($n=7$) and memory-rich hNOJ (IR−) mice at ≥12 wk post-transplantation ($n=8$), based on the percentage of each individual $CD4^+$ T cell subsets at pre-challenge. (A) Weekly analysis of the plasma viral load. Individual hNOJ (IR−) mice are denoted by different colors in this and in the following figures. (B) The plasma viral load at 1 wk post-challenge. Data are plotted individually along with the mean (black lines). Significant differences ($^*P<0.05$, $^{**}P<0.01$) between hNOJ (IR+) mice ($n=7$) and hNOJ (IR−) mice in which the plasma viral

load was detectable (>5000 VL, $n=6$) or all hNOJ (IR−) mice ($n=8$) were determined by the Mann-Whitney U test. (C) The absolute number of $CD4^+$ T cells in the peripheral blood at pre-challenge [hNOJ (IR+) mice; $n=7$ and hNOJ (IR−) mice; $n=8$]. Each $CD4^+$ T cell subset (Naïve, CM, and EM) was defined as outlined in the legend to Figure 6. Data are plotted individually along with the mean (black lines). Significant differences ($^{**}P<0.01$, $^{***}P<0.001$) were determined by the Mann-Whitney U test. (D) The peak plasma viral load during 5 wk post-challenge [hNOJ (IR+) mice; $n=6$ and hNOJ (IR−) mice; $n=7$]. Data are plotted individually along with the mean (black lines). Significant differences ($^{**}P<0.01$) were determined by the Mann-Whitney U test.
doi:10.1371/journal.pone.0053495.g007

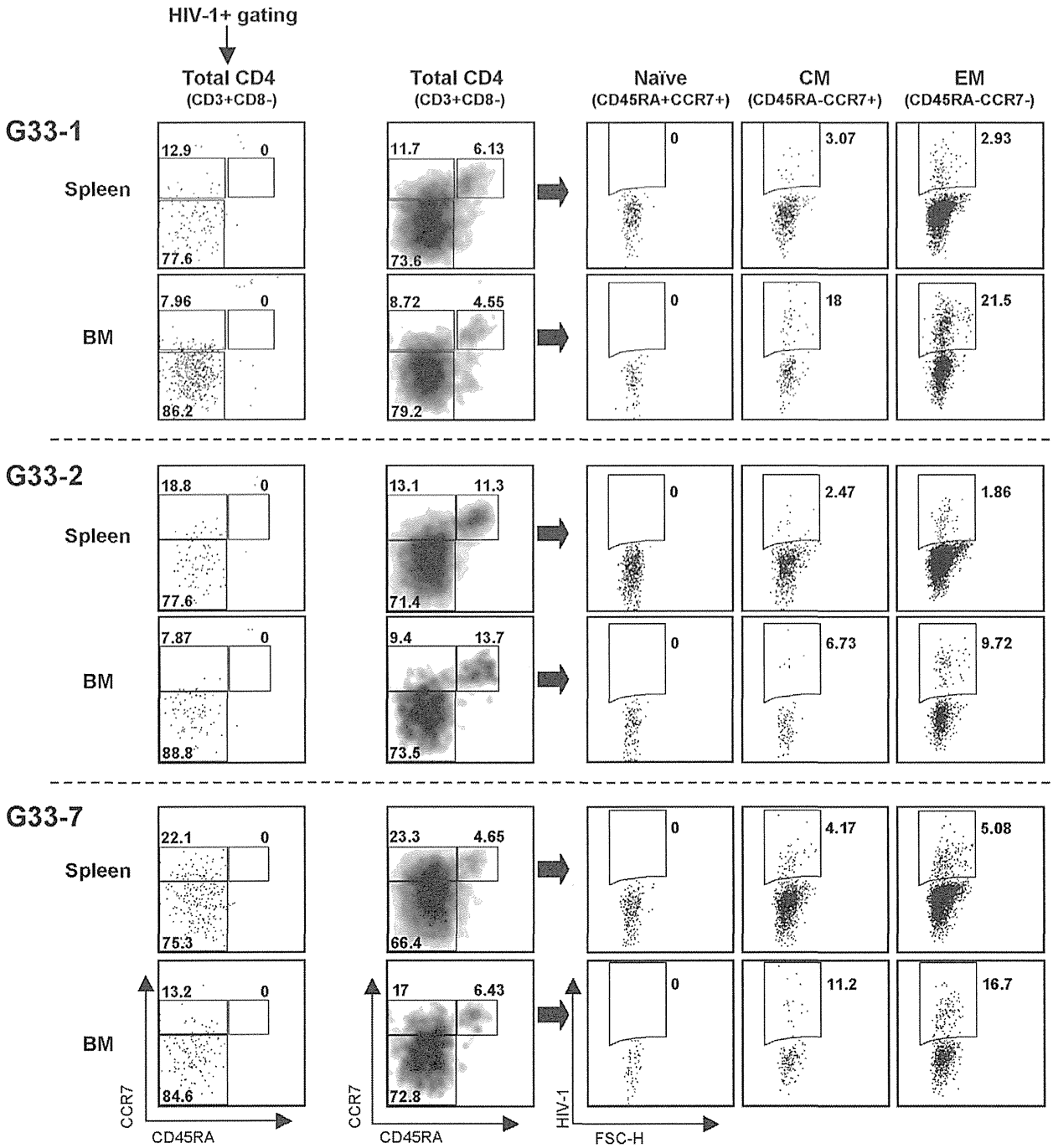

Figure 8. Identification of R5 HIV-1-infected cells in hNOJ mice. Three hNOJ (IR−) mice (G33-1, G33-2, and G33-7), all at 13 wk post-transplantation, were challenged intravenously with $HIV\text{-}1_{NL\text{-}AD8\text{-}D}$. At 2 wk post-challenge, the mice were sacrificed and the infected cells in the spleens and BM were analyzed by flow cytometry. Each $CD4^+$ T cell subset (Naïve, CM, or EM) was defined as outlined in the legend to Figure 6. Infected cells were identified based on their expression of the fluorescent reporter, DsRed.
doi:10.1371/journal.pone.0053495.g008

cells were rendered $CD3^+CD8^-$ cells in order to include CD4-downmodulated HIV-1-infected cells. When analyzing the spleens and BM, we detected infected cells within the CM and EM subsets, but not within the naïve subset. The majority of the infected cells were within the EM subset, mainly because the EM subset was the most numerous among the $CD4^+$ T cells ($CD3^+CD8^-$ cells) in both the spleens and BM at 2 wk post-challenge. However, the percentage of infected cells within the CM and EM subsets was identical. These results indicate that both the CM and EM subsets are a target of R5 HIV-1 *in vivo*.

Discussion

NOJ mice were recently developed as an alternative recipient mouse strain for the construction of humanized mice [18]. This novel strain was used in the present study. Since the Janus family tyrosine kinase, Jak3, mediates downstream signaling from the common γ chain, and is responsible for lymphocytes development [46], the phenotype of NOJ mice, which lack the *Jak3* gene, is the same as that of NOG/NSG mice [18]. Various methods are used to construct conventional humanized mouse models; however, the different methods may result in different outcomes in terms of hematopoietic cell development. Therefore, to make the experiment easier and more effective as previously suggested [9], we constructed humanized NOJ mice by transplanting $CD34^+$ HSCs isolated from umbilical cord blood into the liver of newborn mice. The present study used hNOJ mice that were not irradiated prior to HSC transplantation (i.e., hNOJ (IR−) mice), in comparison with irradiation-treated hNOJ mice (i.e., hNOJ (IR+) mice) that have been already established [18,47,48]. Each hematopoietic cell population, such as T cells, B cells, monocytes, and dendritic cells in irradiation-treated hNOJ mice show the same developmental characteristics [18,47,48] as those in other conventional humanized mouse models constructed with different strains using the same method (newborn mice were irradiated prior to intrahepatic transplantation of umbilical cord blood-derived HSCs) [16,17,49]. Therefore, hNOJ mice may be an alternative humanized mouse model, and experimental data pertaining to these hNOJ mice may be shared with other conventional humanized mouse models. However, an obvious difference between NOJ mice and other strains is their susceptibility to irradiation, which means that they have a limited life-span.

To evaluate hNOJ mice as an experimental animal model of HIV-1 infection, we first investigated how the degree of reconstitution affects the cellularity and development of $CD4^+$ T cells using hNOJ (IR+) and (IR−) mice, which represent high and low chimerism groups, respectively. However, we found that qualitative differences in the characteristics of the reconstituted $CD4^+$ T cells, such as the process of differentiation, the degree of activation, and CCR5/CXCR4 expression, were similar between hNOJ (IR+) and hNOJ (IR−) mice at least during the first 16 wk post-transplantation. In hNOJ mice, the cellularity of $CD4^+$ T cells and proportion of each $CD4^+$ T cell subset within the peripheral blood were similar to those in other organs, such as the spleen and BM (Figure 4B and data not shown), suggesting that the peripheral blood $CD4^+$ T cell population may be representative of the $CD4^+$ T cell distribution throughout other systemic compartments in these mice. In humans, the $CD45RA^+CCR7^+$ naïve and $CD45RA^-CCR7^-$ EM subsets of $CD4^+$ T cells constitute the major subset within the peripheral blood and spleen, respectively [50]. The most striking difference in the $CD4^+$ T cells between hNOJ mice and humans noted here was that hNOJ mice showed a higher percentage of $CD4^+$ T cells expressing HLA-DR, Ki-67, and CCR5 during the later phase post-transplantation.

The memory subset (either CD45RA-negative or CD45RO-positive) tends to increase with time in conventional humanized mice [28,51,52]. We found that the expansion of the $CD45RA^-CCR7^-CD27^+$ EM_{early} and $CD45RA^-CCR7^-CD27^-$ $EM_{int/late}$ subsets, but not that of the $CD45RA^-CCR7^+CD27^+$ CM subset, was associated with an activated phenotype. As suggested elsewhere [27,28], this is probably due to the occurrence of HSP, particularly HPE-type HSP, because (1) memory subsets, particularly the $EM_{int/late}$ subset, expressed the proliferation marker, Ki-67, at higher levels than the naïve subset, and the levels were much higher than those expressed by the $EM_{int/late}$ subset within human PBMC population; (2) the $EM_{int/late}$ subset showed the greatest IFN-γ-producing capacity; and (3) IL-2, IL-7, and IL-15 were undetectable in the plasma when $CD4^+$ T cells converted to an activated memory phenotype.

HPE-type HSP requires TCR-dependent antigen recognition, which is independent of IL-7 [25,26]. In line with this, Onoe *et al.* demonstrated that HPE-type HSP of $CD4^+$ T cells correlated with the percentage of $CD14^+$ monocytes in the periphery when autologous T cells reconstituted in BLT mice were adoptively transferred into T cell-deficient humanized NOD/SCID mice and suggested that $CD4^+$ T cells need to interact with self MHC-II molecules expressed by autologous myeloid-derived antigen-presenting cells (APCs) to drive their expansion [26]. Furthermore, Suzuki *et al.* used a humanized mouse model based upon HLA-DR-transgenic NOG sub-strain mice to show that expansion of the EM subset of $CD4^+$ T cells occurs in an MHC-II (HLA-DR)-dependent manner [28]. In the present study, hNOJ (IR+) mice showed a significantly higher proportion of $CD14^+$ monocytes within the PBMC population, and developed more $CD4^+$ T cells than hNOJ (IR−) mice. Although we did not examine the proportion of APCs in hNOJ (IR+) or hNOJ (IR−) mice in the present study, it is conceivable that hNOJ (IR+) mice have more APCs due to the higher level of chimerism. Therefore, TCR-dependent antigen recognition via myeloid-derived APCs may enhance HPE-type HSP of reconstituted $CD4^+$ T cells in hNOJ (IR+) mice.

The main aim of this study was to examine whether, and how, HIV-1 infectivity is affected in different humanized mouse models in which the $CD4^+$ T cell composition is qualitatively and/or quantitatively different, e.g., naïve- or memory-rich phenotypes. The results showed that the infectivity of R5 HIV-1 was different between the naïve-rich and memory-rich mouse groups. One of the most noticeable differences between the two mouse groups was that the plasma viral load at 1 wk post-challenge was significantly higher in naïve-rich hNOJ (IR+) mice than it was in memory-rich hNOJ (IR−) mice. Although robust plasma viral loads have been reported in other conventional humanized mouse models of R5 HIV-1 infection even at 1 wk post-challenge [17,53,54], our result may be curious because the R5 HIV-1 infectivity of naïve $CD4^+$ T cells is very low, and because naïve-rich hNOJ (IR+) mice would have few memory $CD4^+$ T cells compared with memory-rich hNOJ (IR−) mice. In the present study, we could not determine which cellular parameters pertaining to $CD4^+$ T cells at pre-challenge were associated with the initial plasma viral load; therefore, the reason for the difference in viral load remains unclear. One possibility may be the different proportions of dendritic cells present in hNOJ (IR+) and hNOJ (IR−) mice, since HIV-1 transmission/dissemination efficiently occurs via dendritic cell-$CD4^+$ T cell contact [3,55,56,57]. This needs to be clarified in future studies.

Another noticeable difference between naïve-rich hNOJ (IR+) and memory-rich hNOJ (IR−) mice in terms of the viral infection

was the peak level of the plasma viral load. Memory-rich hNOJ (IR−) mice showed a markedly higher peak level of the plasma viral load during 5 wk post-challenge, suggesting the contribution of the memory $CD4^+$ T cell subset in this setting. Notably, Nie *et al.* showed massive infection of the $CD45RA^-CD45RO^+CCR7^-$ EM subset by R5 HIV-1 in NOG-background humanized mice [51]. Likewise, when we analyzed the spleens and BM from hNOJ (IR−) mice at 2 wk post-challenge with R5 HIV-1, the majority of infected cells were present in the EM subset, most likely because the EM subset was the most numerous at that time. However, when individual subsets were analyzed carefully, the percentage of infected cells in the CM and EM subsets was similar. This is explained by the fact that the fusion efficiency of R5 HIV-1 was comparable between the two subsets (Figure 6E). Taken together, the data obtained in the present study suggest that the CM subset plays a role as both a target and a reservoir for R5 HIV-1 in an HIV-1 infected humanized NOJ mouse model.

hNOJ (IR+) and hNOJ (IR−) mice were highly permissive for infection with both CCR5-tropic HIV-1 (Figures 7 and 8) and CXCR4-tropic HIV-1 (data not shown). However, because hNOJ (IR+) mice have such a short life-span due to irradiation, their use is restricted to the early phase post-transplantation; their use, therefore, is restricted to the study of short-term of HIV-1 infection. By contrast, hNOJ (IR−) mice would be useful for longitudinal analyses of HIV-1 infection, as shown by other studies that used other conventional humanized mouse models [22,53,58]. However, it should be noted that level of HIV-1 infectivity would change, depending on the cellularity of the reconstituted $CD4^+$ T cells in hNOJ mice. Therefore, the selective use of humanized mice according to the disease model is important. For instance, hNOJ mice at the early phase post-transplantation would be a useful model for healthy young humans, in which the naïve $CD4^+$ T cell subset is relatively rich [59,60,61]. On the other hand, hNOJ mice at the late phase post-transplantation (i.e., hNOJ (IR−) mice), might be more suitable as a model for Immune Reconstitution Inflammatory Syndrome, which involves an activated $CD4^+$ T cell burst during post anti-retro viral therapy in HIV-infected individuals [62].

In conclusion, although no obvious differences in the cellularity of $CD4^+$ T cells were found between hNOJ (IR+) and hNOJ (IR−) mice, at least within 16 wk post-transplantation, reconstituted $CD4^+$ T cells converted to an activated memory phenotype over time. The infectivity of R5 HIV-1 was modulated *in vivo* in these humanized mice, depending on the percentage of memory $CD4^+$ T cells. Therefore, the present study suggests that humanized mouse models should be used selectively according to the experimental objectives, taking into account different human physiological states, to gain an appropriate understanding of HIV-1 infection/pathogenesis.

Acknowledgments

We thank Drs. Naoki Yamamoto and Satoru Watanabe (National University of Singapore, Singapore) for helpful advice regarding the construction of humanized mice, Dr. Minoru Tobiume (NIID, Japan) for providing pMM310, Dr. Takuya Yamamoto (National Institutes of Health, USA) for valuable discussion and Ms. Kaori Okano (our laboratory) for technical support. We also thank the Tokyo Cord Blood Bank for providing human umbilical cord blood and the Blood Bank of Japan Red Cross for providing adult human peripheral blood.

Author Contributions

Conceived and designed the experiments: KT YTY. Performed the experiments: KT MI SI YYM. Analyzed the data: KT MI SO KK YTY. Contributed reagents/materials/analysis tools: SO. Wrote the paper: KT. Edited the paper: KK YTY.

References

1. Berger EA, Murphy PM, Farber JM (1999) Chemokine receptors as HIV-1 coreceptors: roles in viral entry, tropism, and disease. Annu Rev Immunol 17: 657–700.
2. McClure MO, Sattentau QJ, Beverley PC, Hearn JP, Fitzgerald AK, et al. (1987) HIV infection of primate lymphocytes and conservation of the CD4 receptor. Nature 330: 487–489.
3. Tsunetsugu-Yokota Y (2008) Transmission of HIV from dendritic cells to $CD4^+$ T cells: a promising target for vaccination and therapeutic intervention. In: Kendow LB, editor. AIDS Vaccines, HIV Receptors and AIDS Research. New York: Nova Science Publishers, Inc. 117–128.
4. Picker LJ, Watkins DI (2005) HIV pathogenesis: the first cut is the deepest. Nat Immunol 6: 430–432.
5. Simon V, Ho DD (2003) HIV-1 dynamics in vivo: implications for therapy. Nat Rev Microbiol 1: 181–190.
6. Stevenson M (2003) HIV-1 pathogenesis. Nat Med 9: 853–860.
7. Goldstein H (2008) Summary of presentations at the NIH/NIAID New Humanized Rodent Models 2007 Workshop. AIDS Res Ther 5: 3.
8. Legrand N, Ploss A, Balling R, Becker PD, Borsotti C, et al. (2009) Humanized mice for modeling human infectious disease: challenges, progress, and outlook. Cell Host Microbe 6: 5–9.
9. Legrand N, Weijer K, Spits H (2006) Experimental models to study development and function of the human immune system in vivo. J Immunol 176: 2053–2058.
10. Manz MG (2007) Human-hemato-lymphoid-system mice: opportunities and challenges. Immunity 26: 537–541.
11. Shacklett BL (2008) Can the new humanized mouse model give HIV research a boost. PLoS Med 5: e13.
12. Sato K, Koyanagi Y (2011) The mouse is out of the bag: insights and perspectives on HIV-1-infected humanized mouse models. Exp Biol Med (Maywood).
13. Wege AK, Melkus MW, Denton PW, Estes JD, Garcia JV (2008) Functional and phenotypic characterization of the humanized BLT mouse model. Curr Top Microbiol Immunol 324: 149–165.
14. Berges BK, Rowan MR (2011) The utility of the new generation of humanized mice to study HIV-1 infection: transmission, prevention, pathogenesis, and treatment. Retrovirology 8: 65.
15. Ito R, Takahashi T, Katano I, Ito M (2012) Current advances in humanized mouse models. Cell Mol Immunol. 9: 208–214.
16. Traggiai E, Chicha L, Mazzucchelli L, Bronz L, Piffaretti JC, et al. (2004) Development of a human adaptive immune system in cord blood cell-transplanted mice. Science 304: 104–107.
17. Akkina R, Berges BK, Palmer BE, Remling L, Neff CP, et al. (2011) Humanized $Rag1^{-/-}\gamma c^{-/-}$ mice support multilineage hematopoiesis and are susceptible to HIV-1 infection via systemic and vaginal routes. PLoS One 6: e20169.
18. Okada S, Harada H, Ito T, Saito T, Suzu S (2008) Early development of human hematopoietic and acquired immune systems in new born NOD/Scid/$Jak3^{null}$ mice intrahepatic engrafted with cord blood-derived $CD34^+$ cells. Int J Hematol 88: 476–482.
19. Shultz LD, Ishikawa F, Greiner DL (2007) Humanized mice in translational biomedical research. Nat Rev Immunol 7: 118–130.
20. Liu C, Chen BJ, Deoliveira D, Sempowski GD, Chao NJ, et al. (2010) Progenitor cell dose determines the pace and completeness of engraftment in a xenograft model for cord blood transplantation. Blood 116: 5518–5527.
21. Singh M, Singh P, Gaudray G, Musumeci L, Thielen C, et al. (2012) An improved protocol for efficient engraftment in NOD/LTSZ-SCIDIL-$2R\gamma^{NULL}$ mice allows HIV replication and development of anti-HIV immune responses. PLoS One 7: e38491.
22. Watanabe S, Ohta S, Yajima M, Terashima K, Ito M, et al. (2007) Humanized NOD/SCID/IL2$R\gamma^{null}$ mice transplanted with hematopoietic stem cells under nonmyeloablative conditions show prolonged life spans and allow detailed analysis of human immunodeficiency virus type 1 pathogenesis. J Virol 81: 13259–13264.
23. Gorantla S, Sneller H, Walters L, Sharp JG, Pirruccello SJ, et al. (2007) Human immunodeficiency virus type 1 pathobiology studied in humanized BALB/c-$Rag2^{-/-}\gamma_c^{-/-}$ mice. J Virol 81: 2700–2712.
24. Boyman O, Letourneau S, Krieg C, Sprent J (2009) Homeostatic proliferation and survival of naive and memory T cells. Eur J Immunol 39: 2088–2094.
25. Min B, Yamane H, Hu-Li J, Paul WE (2005) Spontaneous and homeostatic proliferation of CD4 T cells are regulated by different mechanisms. J Immunol 174: 6039–6044.
26. Onoe T, Kalscheuer H, Chittenden M, Zhao G, Yang YG, et al. (2010) Homeostatic expansion and phenotypic conversion of human T cells depend on peripheral interactions with APCs. J Immunol 184: 6756–6765.

27. Legrand N, Cupedo T, van Lent AU, Ebeli MJ, Weijer K, et al. (2006) Transient accumulation of human mature thymocytes and regulatory T cells with CD28 superagonist in "human immune system" *Rag2*$^{-/-}\gamma_c^{-/-}$ mice. Blood 108: 238–245.
28. Suzuki M, Takahashi T, Katano I, Ito R, Ito M, et al. (2012) Induction of human humoral immune responses in a novel HLA-DR-expressing transgenic NOD/Shi-scid/γc^{null} mouse. Int Immunol 24: 243–252.
29. Yamamoto T, Tsunetsugu-Yokota Y, Mitsuki YY, Mizukoshi F, Tsuchiya T, et al. (2009) Selective transmission of R5 HIV-1 over X4 HIV-1 at the dendritic cell-T cell infectious synapse is determined by the T cell activation state. PLoS Pathog 5: e1000279.
30. Kemp K, Bruunsgaard H (2001) Identification of IFN-γ-producing CD4$^+$ T cells following PMA stimulation. J Interferon Cytokine Res 21: 503–506.
31. Cavrois M, De Noronha C, Greene WC (2002) A sensitive and specific enzyme-based assay detecting HIV-1 virion fusion in primary T lymphocytes. Nat Biotechnol 20: 1151–1154.
32. Dai J, Agosto LM, Baytop C, Yu JJ, Pace MJ, et al. (2009) Human immunodeficiency virus integrates directly into naive resting CD4$^+$ T cells but enters naive cells less efficiently than memory cells. J Virol 83: 4528–4537.
33. Tobiume M, Lineberger JE, Lundquist CA, Miller MD, Aiken C (2003) Nef does not affect the efficiency of human immunodeficiency virus type 1 fusion with target cells. J Virol 77: 10645–10650.
34. O'Doherty U, Swiggard WJ, Malim MH (2000) Human immunodeficiency virus type 1 spinoculation enhances infection through virus binding. J Virol 74: 10074–10080.
35. Saito A, Nomaguchi M, Iijima S, Kuroishi A, Yoshida T, et al. (2010) Improved capacity of a monkey-tropic HIV-1 derivative to replicate in cynomolgus monkeys with minimal modifications. Microbes Infect 13: 58–64.
36. Hiramatsu H, Nishikomori R, Heike T, Ito M, Kobayashi K, et al. (2003) Complete reconstitution of human lymphocytes from cord blood CD34$^+$ cells using the NOD/SCID/γ_c^{null} mice model. Blood 102: 873–880.
37. Yahata T, Ando K, Nakamura Y, Ueyama Y, Shimamura K, et al. (2002) Functional human T lymphocyte development from cord blood CD34$^+$ cells in nonobese diabetic/Shi-*scid*, IL-2 receptor γ null mice. J Immunol 169: 204–209.
38. Okada R, Kondo T, Matsuki F, Takata H, Takiguchi M (2008) Phenotypic classification of human CD4$^+$ T cell subsets and their differentiation. Int Immunol 20: 1189–1199.
39. Seder RA, Darrah PA, Roederer M (2008) T-cell quality in memory and protection: implications for vaccine design. Nat Rev Immunol 8: 247–258.
40. Yue FY, Kovacs CM, Dimayuga RC, Parks P, Ostrowski MA (2004) HIV-1-specific memory CD4$^+$ T cells are phenotypically less mature than cytomegalovirus-specific memory CD4$^+$ T cells. J Immunol 172: 2476–2486.
41. Chomont N, El-Far M, Ancuta P, Trautmann L, Procopio FA, et al. (2009) HIV reservoir size and persistence are driven by T cell survival and homeostatic proliferation. Nat Med 15: 893–900.
42. Surh CD, Sprent J (2008) Homeostasis of naive and memory T cells. Immunity 29: 848–862.
43. Okoye A, Meier-Schellersheim M, Brenchley JM, Hagen SI, Walker JM, et al. (2007) Progressive CD4$^+$ central memory T cell decline results in CD4$^+$ effector memory insufficiency and overt disease in chronic SIV infection. J Exp Med 204: 2171–2185.
44. Mattapallil JJ, Douek DC, Hill B, Nishimura Y, Martin M, et al. (2005) Massive infection and loss of memory CD4$^+$ T cells in multiple tissues during acute SIV infection. Nature 434: 1093–1097.
45. Terahara K, Yamamoto T, Mitsuki YY, Shibusawa K, Ishige M, et al. (2012) Fluorescent Reporter Signals, EGFP, and DsRed, Encoded in HIV-1 Facilitate the Detection of Productively Infected Cells and Cell-Associated Viral Replication Levels. Front Microbiol 2: 280.
46. Park SY, Saijo K, Takahashi T, Osawa M, Arase H, et al. (1995) Developmental defects of lymphoid cells in Jak3 kinase-deficient mice. Immunity 3: 771–782.
47. Sato Y, Takata H, Kobayashi N, Nagata S, Nakagata N, et al. (2010) Failure of effector function of human CD8$^+$ T Cells in NOD/SCID/JAK3$^{-/-}$ immunodeficient mice transplanted with human CD34$^+$ hematopoietic stem cells. PLoS One 5: e13109.
48. Sato Y, Nagata S, Takiguchi M (2012) Effective elicitation of human effector CD8$^+$ T cells in HLA-B*51:01 transgenic humanized mice after infection with HIV-1. PLoS One 7: e42776.
49. Baenziger S, Tussiwand R, Schlaepfer E, Mazzucchelli L, Heikenwalder M, et al. (2006) Disseminated and sustained HIV infection in CD34$^+$ cord blood cell-transplanted Rag2$^{-/-}\gamma_c^{-/-}$ mice. Proc Natl Acad Sci U S A 103: 15951–15956.
50. Langeveld M, Gamadia LE, ten Berge IJ (2006) T-lymphocyte subset distribution in human spleen. Eur J Clin Invest 36: 250–256.
51. Nie C, Sato K, Misawa N, Kitayama H, Fujino H, et al. (2009) Selective infection of CD4$^+$ effector memory T lymphocytes leads to preferential depletion of memory T lymphocytes in R5 HIV-1-infected humanized NOD/SCID/IL-2Rγ^{null} mice. Virology 394: 64–72.
52. André MC, Erbacher A, Gille C, Schmauke V, Goecke B, et al. (2010) Long-term human CD34$^+$ stem cell-engrafted nonobese diabetic/SCID/IL-2Rγ^{null} mice show impaired CD8$^+$ T cell maintenance and a functional arrest of immature NK cells. J Immunol 185: 2710–2720.
53. Berges BK, Akkina SR, Remling L, Akkina R (2010) Humanized Rag2$^{-/-}\gamma c^{-/-}$ (RAG-hu) mice can sustain long-term chronic HIV-1 infection lasting more than a year. Virology 397: 100–103.
54. Zhang L, Kovalev GI, Su L (2007) HIV-1 infection and pathogenesis in a novel humanized mouse model. Blood 109: 2978–2981.
55. Tsunetsugu-Yokota Y, Yasuda S, Sugimoto A, Yagi T, Azuma M, et al. (1997) Efficient virus transmission from dendritic cells to CD4$^+$ T cells in response to antigen depends on close contact through adhesion molecules. Virology 239: 259–268.
56. David SA, Smith MS, Lopez GJ, Adany I, Mukherjee S, et al. (2001) Selective transmission of R5-tropic HIV type 1 from dendritic cells to resting CD4$^+$ T cells. AIDS Res Hum Retroviruses 17: 59–68.
57. Granelli-Piperno A, Delgado E, Finkel V, Paxton W, Steinman RM (1998) Immature dendritic cells selectively replicate macrophagetropic (M-tropic) human immunodeficiency virus type 1, while mature cells efficiently transmit both M- and T-tropic virus to T cells. J Virol 72: 2733–2737.
58. Nischang M, Sutmuller R, Gers-Huber G, Audige A, Li D, et al. (2012) Humanized mice recapitulate key features of HIV-1 infection: a novel concept using long-acting anti-retroviral drugs for treating HIV-1. PLoS One 7: e38853.
59. Ponnappan S, Ponnappan U (2011) Aging and immune function: molecular mechanisms to interventions. Antioxid Redox Signal 14: 1551–1585.
60. Goronzy JJ, Lee WW, Weyand CM (2007) Aging and T-cell diversity. Exp Gerontol 42: 400–406.
61. Woodland DL, Blackman MA (2006) Immunity and age: living in the past? Trends Immunol 27: 303–307.
62. Lipman M, Breen R (2006) Immune reconstitution inflammatory syndrome in HIV. Curr Opin Infect Dis 19: 20–25.

Jpn. J. Infect. Dis., 66, 207-215, 2013

Original Article

Multicolor Flow Cytometric Analyses of CD4$^+$ T Cell Responses to *Mycobacterium tuberculosis*-Related Latent Antigens

Yoshiro Yamashita[1], Yoshihiko Hoshino[2], Mayuko Oka[4], Sokichi Matsumoto[5], Haruyuki Ariga[6], Hideaki Nagai[6], Masahiko Makino[2], Koya Ariyoshi[1], and Yasuko Tsunetsugu-Yokota[3]*

[1]*Department of Clinical Medicine, Institute of Tropical Medicine, Nagasaki University, Nagasaki 852-8523;*
[2]*Department of Mycobacteriology, Leprosy Research Center, National Institute of Infectious Diseases, Tokyo 189-0002;*
[3]*Department of Immunology, National Institute of Infectious Diseases, Tokyo 162-8640;*
[4]*Division of Applied Life Science, Graduate School of Life and Environmental Sciences, Kyoto Prefectural University, Kyoto 606-8522;*
[5]*Department of Bacteriology, Osaka City University Graduate School of Medicine, Osaka 545-8585; and*
[6]*Center for Respiratory Medicine, National Hospital Organization Tokyo National Hospital, Tokyo 204-8585, Japan*

(Received November 21, 2012. Accepted March 15, 2013)

SUMMARY: Although IFN-γ release assays (IGRAs) provide increased specificity over tuberculin skin tests, the early and sensitive detection of reactivation of latently infected *Mycobacterium tuberculosis* is required to control tuberculosis (TB). Recently, a multicolor flow cytometry has been developed to study CD4$^+$ T cell cytokine responses (IFN-γ/IL-2/TNF-α) to purified protein derivatives (PPD) and *M. tuberculosis*-specific antigens (ESAT-6/CFP-10) and provided useful information regarding anti-TB immunity. However, the diagnostic relevancy remains uncertain. Here, we analyzed three additional CD4$^+$ T cell cytokine responses (IL-10/IL-13/IL-17) to latent mycobacterial antigens (α-crystallin, methylated heparin-binding hemagglutinin [HBHA], and mycobacterial DNA-binding protein 1 [MDP-1]) as well as PPD and ESAT-6/CFP-10 in 12 IGRA$^+$ TB cases and 8 healthy controls. No significant difference in IFN-γ response was observed between TB cases and controls, which was likely due to the high variation among the individuals. However, we found a significant increase over healthy controls in (i) the IL-2 response to HBHA in recovery stage TB cases, (ii) the number of *M. tuberculosis*-specific polyfunctional CD4$^+$ T cells in on-treatment and recovery stage cases, and (iii) the IL-17 response to HBHA and MDP-1 in on-treatment and recovery stage cases. These results suggest that a combination of these T cell cytokine parameters could aid in accurate diagnosis of latent TB infection.

INTRODUCTION

Tuberculosis (TB) is caused by *Mycobacterium tuberculosis* infection. *M. tuberculosis* can establish a long-term persistent infection without causing any symptoms; this condition is referred to as latent TB infection (LTBI). It is estimated that one to two billion people worldwide are living with LTBI (1). A minority of people with LTBI develop clinical disease (active TB) when the host TB defense mechanism is altered by poor health conditions such as malnutrition, aging, and immunodeficiency caused by human immunodeficiency virus (HIV) infection (2). The lifetime risk of clinical disease development in LTBI individuals is estimated to be 5–10% (3,4); this group of individuals may benefit from prophylactic treatment. However, because the vast majority of people with LTBI will not develop active TB, it is not practical to treat all LTBI individuals. Therefore, development of a screening method to identify individuals who may benefit from preventative treatment is required.

Clinical IFN-γ release assays (IGRAs) that detect the IFN-γ response to *M. tuberculosis*-specific antigens such as ESAT-6 and CFP-10 have been developed and are widely utilized for the diagnosis of TB because they are more specific than conventional tuberculin skin tests (5). The sensitivity of IGRAs for the detection of active TB is approximately 85%, and the specificities for the detection of active TB and LTBI are greater than 85% and 98–100%, respectively (6); however, the predictive value of IGRAs for the development of active TB from LTBI is only 2.7% (7).

Although ESAT-6 and CFP-10 are the predominant secretory proteins released during the active stage of *M. tuberculosis*, several mycobacterial antigens are known to be associated with the latent stage of *M. tuberculosis* infection. The α-crystallin (Acr) protein is a member of the small heat shock protein family that has chaperone activity in vitro (8). Acr is required for the growth of *M.*

*Corresponding author: Mailing address: Department of Immunology, National Institute of Infectious Diseases, 1-23-1 Toyama, Shinjuku, Tokyo 162-8640, Japan. Tel: +81-3-4582-2716, Fax: +81-3-5285-1156, E-mail: yyokota@nih.go.jp

tuberculosis in cultured macrophages, and its expression increases under hypoxic conditions (9). Heparin-binding hemagglutinin (HBHA) is a protein that functions as an adhesin for epithelial cells (10). Because the transition from the alveolar space to deeper organ sites is a crucial step in the pathogenesis of LTBI, HBHA may serve as a target antigen for the diagnosis of LTBI, as reported previously (11). Mycobacterial DNA-binding protein 1 (MDP-1) belongs to a group of orthologous DNA-binding proteins that constitute 8–10% of total protein in mycobacteria such as *Mycobacterium bovis* bacillus Calmette-Guérin (BCG) and *M. tuberculosis* (12,13). MDP-1 is upregulated in the stationary phase of *M. tuberculocis* infection and induces protective immunity against *M. tuberculosis* infection in mice (12,14). Therefore, in combination with *M. tuberculosis*-specific ESAT-6 and CFP-10, the latency-associated antigens may aid in monitoring the immune response to *M. tuberculosis* in LTBI.

$CD4^+$ T cells produce IFN-γ and play a critical role in controlling persistent *M. tuberculosis* infection. HIV-infected patients with a decreased baseline $CD4^+$ T cell count have a higher incidence of TB (15), and macaques coinfected with *M. tuberculosis* and simian immunodeficiency virus that display a decreased $CD4^+$ T cell count show earlier reactivation of latent *M. tuberculosis* infection (16). There are many subsets of $CD4^+$ T cells, such as T-helper 1 (Th1), Th2, Th17, and regulatory T cells (Tregs), and they produce a unique set of cytokines (17). All $CD4^+$ T subsets cooperate or interfere with each other to control infection, and the dominant subset may differ between active and latent *M. tuberculosis* infection cases. Multi-parameter flow cytometry enables analysis of these cytokine-producing antigen-specific T cells ex vivo. Using this technology, it was proposed that polyfunctional T cells that produce multiple cytokines are associated with protective immunity (18), and T-cell polyfunctionality has been analyzed in individuals with HIV and *M. tuberculosis* double infection (19,20). These studies suggested that the number of *M. tuberculosis*-specific T cells producing a combination of IFN-γ, IL-2, and/or TNF-α may be correlated with the level of *M. tuberculosis* protection; however, evidence that these polyfunctional T cells are directly associated with protection is still lacking. Furthermore, no previously published study has evaluated polyfunctional T cells, including subsets of $CD4^+$ T cells, with a wide range of *M. tuberculosis* antigens such as latent phase proteins.

In this study, we postulated that the profiles of multiple T cell cytokines produced in response to latency-associated antigens vary at distinct clinical stages of *M. tuberculosis* infection and provide diagnostic information that supplements the ESAT-6 and CFP-10 profiles detected by conventional IGRAs. Multicolor flow cytometric analyses of the five $CD4^+$ T cell cytokine responses, such as IFN-γ, IL-2, IL-10, IL-13, and IL-17, to several *M. tuberculosis*-specific antigens, including latency-associated antigens, in active TB (on-treatment), non-active TB (recovery stage and contact cases), and healthy control cases are presented.

MATERIALS AND METHODS

Study subjects: Twelve *M. tuberculosis*-infected cases, including seven cases of TB diagnosed by sputum smear or PCR analysis and five cases with a history of close contact with active TB, were recruited from Tokyo National Hospital (Tokyo, Japan). The characteristics of the *M. tuberculosis*-infected cases, all of which were QuantiFERON TB (QFT) test positive, are shown in Table 1. At the time of evaluation, two of the seven TB cases were receiving on-going treatment with anti-TB drug therapy and five were in the recovery stage after completion of anti-TB drug therapy. One contact case was receiving prophylactic anti-TB treatment.

Table 1. Characteristics of *M. tuberculosis*-infected cases

Case no.	Sex	Age	Anti-TB therapy (duration after treatment)	QFT test	Others
1	male	25	ongoing (6 month)	positive	
2	male	58	none (contact)	positive	
3	male	79	none (contact)	positive	
4	male	53	prophylaxis (contact)	positive	
5	female	82	ongoing (<1 month)	positive	
6	male	31	previous (>6 years)	positive	
7	male	76	previous (>2 years)	positive	
8	male	79	previous (>1 year)	positive	
9	female	36	none (contact)	positive	
10	male	77	previous (>4 years)	positive	HIV+
11	female	46	none (contact)	positive	
12	male	95	previous (>1 year)	positive	

Eight healthy controls with no history of TB infection or exposure, including two males and six females with a mean age of 32.1 years, were recruited from Nagasaki University (Nagasaki, Japan). A blood sample from one of the laboratory staff, who had a previous history of being highly reactive to many mycobacterial antigens without displaying symptoms, was used as a positive control. All the samples included in the present study were obtained with informed consent and with ethical approval from the Institute of Tropical Medicine Nagasaki University Joint Ethics Committee as well as from the research and ethical committees of the National Institute of Infectious Diseases (Tokyo, Japan).

Reagents: Staphylococcal enterotoxin B (SEB) and purified protein derivatives (PPD) of *M. tuberculosis* were purchased from Sigma-Aldrich (St. Louis, Mo., USA) and Japan BCG Laboratory (Tokyo, Japan), respectively.

ESAT-6, CFP-10, Acr, methylated HBHA (mHABA), and methylated MDP-1 (mMDP-1) were recombinant protein products from *Escherichia coli*. The vectors expressing ESAT-6, CFP-10, HBHA, and MDP-1 were produced by a PCR-based approach using a bacterial chromosome. Each PCR product containing the relevant coding region was designed to allow the expression of a C-terminal, 6× histidine-tagged variant of the recombinant protein following ligation into the pET-21b vector (Toyobo, Osaka, Japan). Recombinant *M. tuberculosis* proteins were purified using Ni-NTA columns (1 ml bed volume) (QIAGEN, Germantown, Md., USA), according to the manufacturer's instructions. The endotoxins were excised from recombinant *M. tuberculosis* proteins using EndoTrap columns (Profos AG, Regenburg, Germany), according to the manufacturer's instructions. Residual endotoxin levels

were determined using a Limulus amebocyte lysate test (Lonza, Walkersville, Md., USA) and were found to be below 0.5 EU/10 μg protein. Chemical methylation of the lysine residues in recombinant mHBHA and mMDP-1 was performed as described previously (21).

The following fluorescently labeled monoclonal antibodies (mAbs) were used in this study: anti-CD3-APC-Cy7 (HIT3a), anti-IFN-γ-PE-Cy7 (4S.B3), anti-IL-10-PE (JES3-9D7), anti-IL-17-Alexa Fluor 700 (BL168), anti-TNF-α-PerCP-Cy5.5 (MAb11) (Biolegend, San Diego, Calif., USA), anti-CD4-Pacific Blue (OKT4), anti-IL-2-APC (MQ1-17H12), and anti-IL-13- FITC (PVM13-1) (eBioscience, San Diego, Calif., USA). Where necessary, the relevant isotype control mAb was used. Cell viability was assessed using the LIVE/DEAD kit (Invitrogen, Carlsbad, Calif., USA). Brefeldin-A (BFA) was purchased from Sigma-Aldrich.

In vitro culture: Peripheral blood mononuclear cells (PBMCs) were isolated from 10 ml of heparinized blood by density gradient centrifugation using Lymphoprep solution (AXIS-Shield, Oslo, Norway). After two washes with PBS, cells were resuspended in R10 medium, consisting of RPMI 1640 (Wako Junyaku Co., Tokyo, Japan) supplemented with 10% FBS, penicillin/streptomycin (Invitrogen), and 2 mM L-glutamine. A total of 0.5 to 1 $\times$ 10^6 PBMCs in 200 μl of R10 medium were plated into each well of a 96-well round bottom culture plate. Cultures were incubated with no antigen (medium only) or medium containing SEB (16.7 μg/ml), PPD (25 μg/ml), ESAT-6 and CFP-10 (0.9 μg/ml each), Acr (1.4 μg/ml), mHBHA (1.8 μg/ml), or mMDP-1 (7.5 μg/ml). All antigen stimulations were performed in the presence of BFA (1 μg/ml). The cells were incubated overnight (14–16 h) at 37°C in a 5% CO_2 incubator.

Flow cytometry: Following overnight incubation, the culture plate was centrifuged and the supernatant was removed. This was followed by the addition of 20 μl of a previously titrated surface marker cocktail (CD3 and CD4) and LIVE/DEAD reagent. The plate was vortexed and incubated for 30 min at 4°C. After washing with PBS, the cells were permeabilized, fixed with FACS permeabilizing solution (BD Bioscience, San Jose, Calif., USA), and incubated for 20 min at 4°C. The cells were washed three times with Perm/wash solution (BD Bioscience), and 20 μl of a previously titrated anti-cytokine mAbs cocktail containing IFN-γ, IL-2, IL-10, IL-13, and IL-17 was then added. After 30-min incubation at 4°C, the cells were washed and acquired using a FACS Canto II flow cytometer (BD Bioscience). FACS data were reanalyzed using FlowJo software, version 8.8.7 (TreeStar, San Carlos, Calif., USA).

Statistical analysis: Group medians and distributions were analyzed using Wilcoxon matched-pairs signed-rank tests and Mann-Whitney *U* tests. All analyses were performed using GraphPad Prism software, version 5 (San Diego, Calif., USA). A P value $<0.05\%$ was considered significant.

RESULTS

Assessment of IFN-γ-producing *M. tuberculosis*-specific T cells in fresh and frozen PBMCs: T cells stimulated with recombinant *M. tuberculosis*-related antigens were analyzed by flow cytometry. Because the majority of the Japanese population is immunized with BCG in early childhood, many individuals produce PPD-reactive memory T cells. Interestingly, one asymptomatic volunteer was found to be highly reactive to both PPD and the *M. tuberculosis*-specific antigens, ESAT-6 and CFP-10. This volunteer was a 60-year-old laboratory technician who had worked in a microbiology laboratory for almost 40 years and was therefore at a high risk of *M. tuberculosis* exposure; however, this individual had no history of TB symptoms or signs of respiratory diseases. PBMCs from this individual were used to determine the concentration of *M. tuberculosis*-related antigens required to maximize the T cell response without causing cell toxicity. Because fresh PBMC samples were not always available, levels of several cytokines from both fresh and frozen PBMC samples stimulated with a mixture of ESAT-6 and CFP-10 were compared. Both fresh and frozen PBMCs were stimulated with an ESAT-6/CFP-10 mixture (1.5 μg each) overnight. T cell surface staining with CD3, CD4, and CD8, followed by intracellular staining, was then performed using a multicolor flow cytometer and mAbs targeting IL-2, TNF-α, MIP-1β, and IL-17. The frequencies of IFN-γ-producing $CD4^+$ and $CD8^+$ T cells in fresh PBMCs (Fig. 1A) were approximately 2% and 3.8%, respectively. These frequencies were reduced by more than 50% in the frozen samples (Fig. 1B). The frequency of MIP-1β-producing $CD8^+$ T cells was decreased from 2.79 + 0.81% (3.6% total) in fresh samples (Fig. 1A) to 1.48 + 0.35% (1.83% total) in frozen samples (Fig. 1B). However, the frequencies of IL-2, TNF-α, and MIP-1β-producing $CD4^+$ T cells were similar in fresh and frozen PBMCs. These results strongly suggest that IFN-γ-producing T cells are susceptible to degradation by freeze-thaw procedures. Therefore, subsequent studies were performed using PBMCs obtained from fresh blood samples.

IFN-γ and IL-2 responses of $CD4^+$ T cells to *M. tuberculosis*-related antigens: The IFN-γ and IL-2 responses of $CD4^+$ T cells to various *M. tuberculosis*-related antigens in the 12 *M. tuberculosis*-infected cases and eight healthy controls were investigated by flow cytometry. Double-positive (IFN-γ and IL-2) $CD4^+$ T cells were detected following PPD and ESAT-6/CFP-10 stimulation; the frequency of these double-positive cells was lower for ESAT-6/CFP-10 stimulation than that for PPD stimulation (Fig. 2A). $CD4^+$ T cell responses to other *M. tuberculosis*-related antigens, namely Acr, mHBHA, and mMDP-1, were also investigated (Fig. 2A). In *M. tuberculosis*-infected cases, the IFN-γ response of $CD4^+$ T cells to all *M. tuberculosis*-related antigens tested was significantly higher than that of control cells exposed to medium alone (Fig. 2B). In contrast, the IFN-γ responses to *M. tuberculosis*-related antigens in healthy controls were not statistically significant (Fig. 2B). The latter finding remained the same even if analysis was confined to individuals with a high $CD4^+$ T cell response to PPD. These results indicate that the *M. tuberculosis*-related antigens used in this study can stimulate *M. tuberculosis*-reactive or mycobacteria-reactive $CD4^+$ T cells. Interestingly, IL-2-producing $CD4^+$ T cells were detectable in the absence of antigen in three *M. tuberculosis*-infected cases; however, none were detected in healthy controls (Fig.

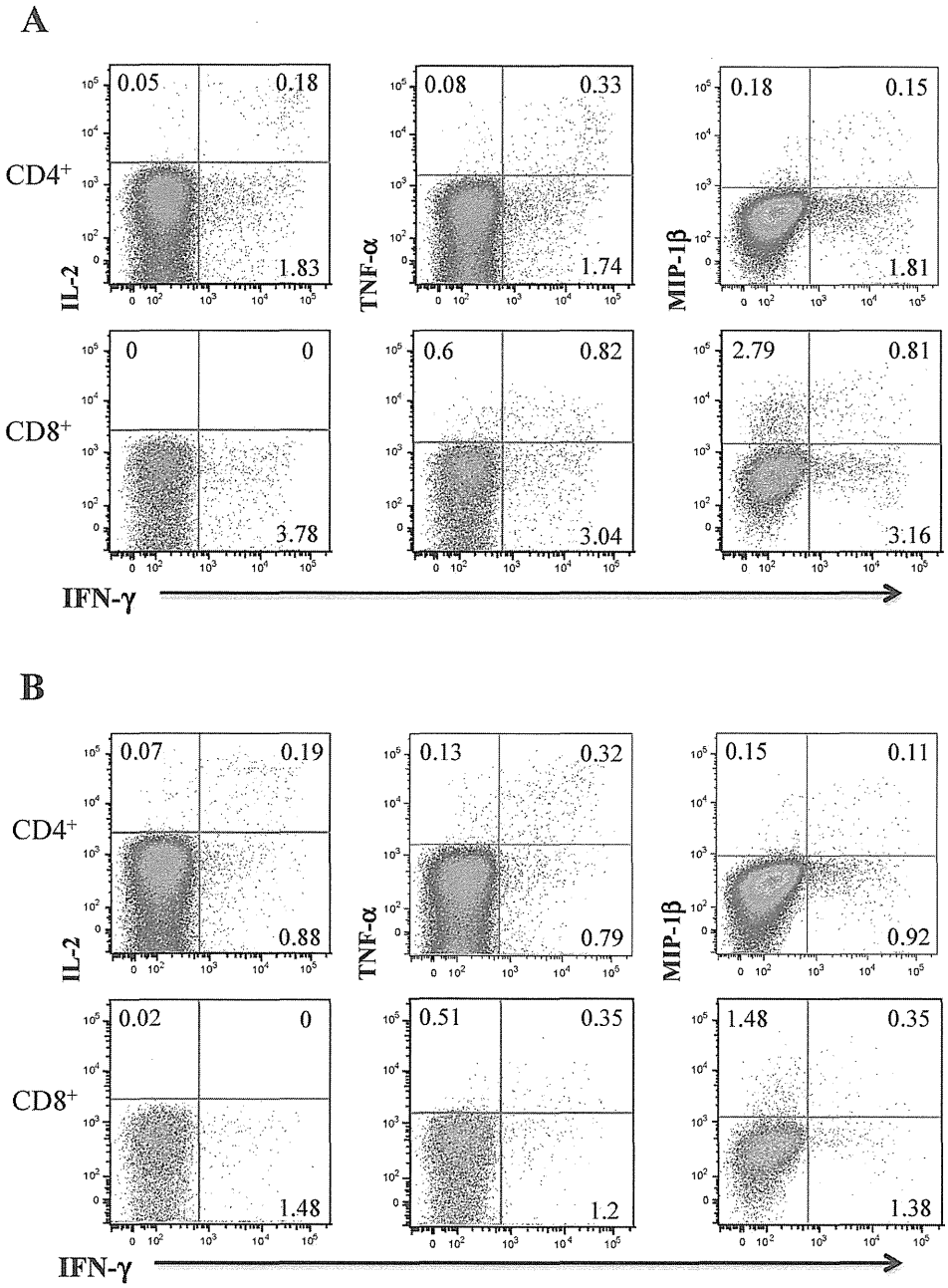

Fig. 1. Flow cytometric analyses of fresh and frozen PBMCs following ESAT-6/CFP-10 stimulation. (A) Fresh PBMCs. (B) Frozen PBMCs. PBMCs were prepared from one asymptomatic high responder. Upper plots display $CD3^+CD4^+$ T cells, and lower plots display $CD3^+CD8^+$ T cells. The plots display the percentage of cells producing IFN-γ and either IL-2, TNF-α, or MIP1-β. Values in the lower right quadrant represent the percentage of IFN-γ-producing cells; values in the upper left quadrant represent the percentage of IL-2, TNF-α, or MIP1-β-producing cells; and values in the upper right quadrant represent the percentage of cells producing both IFN-γ and the relevant cytokine.

2C). Despite this non-specific response, the IL-2 response to PPD in *M. tuberculosis*-infected cases was significantly higher than that of media-exposed control cells ($P = 0.0425$). In healthy controls, a slight IL-2 response to PPD was detected; however, the response was not significant (Fig. 2C). Further analysis of the IL-2 response to mHBHA in *M. tuberculosis*-infected cases grouped by clinical status revealed a significant IL-2 response in recovery stage TB cases compared with that in control cases ($P = 0.0225$, Fig. 2D) and contact cases ($P = 0.0119$, Fig. 2D). Interestingly, two distinct groups were identified, one of which had a high IL-2 response and the other had a low IL-2 response in on-treatment and recovery stage TB cases. This finding suggests that the IL-2-producing $CD4^+$ T cells that are stimulated by mHBHA may indicate ongoing *M. tuberculosis* replication.

Use of polyfunctional $CD4^+$ T cells producing both IFN-γ and IL-2 as an indicator of TB: The polyfunctionality and corresponding high mean fluorescence in-

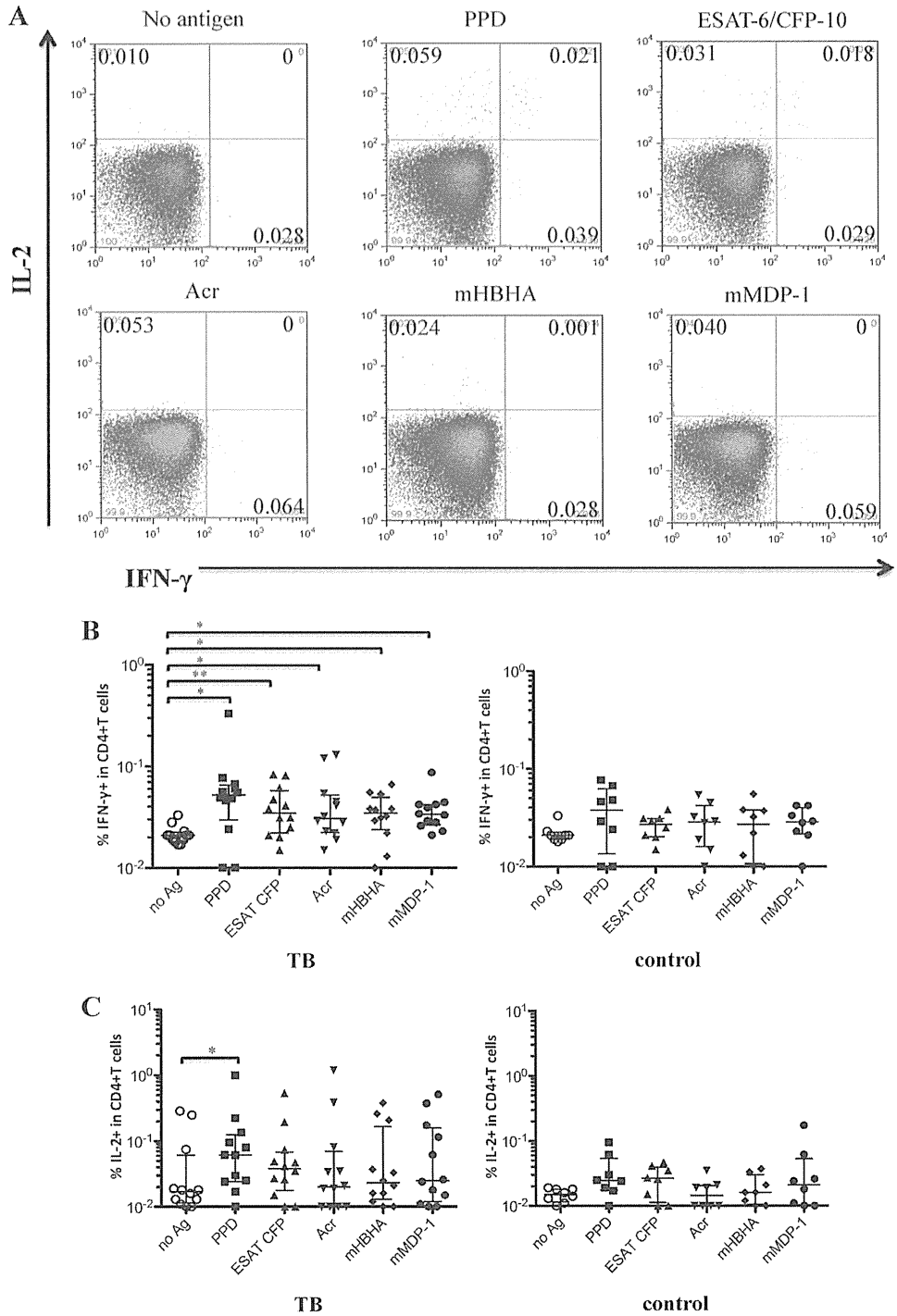

Fig. 2. IFN-γ and IL-2 responses of CD4$^+$ T cells to *M. tuberculosis*-related antigens. (A) Representative flow cytometry results showing IFN-γ and IL-2 responses of CD3$^+$ CD4$^+$ T cells to various *M. tuberculosis*-related antigens. Values in the lower right quadrant represent the percentage of IFN-γ-producing cells, values in the upper left quadrant represent the percentage of IL-2-producing cells, and values in the upper right quadrant represent the percentage of cells producing both IFN-γ and IL-2. IFN-γ (B) and IL-2 (C) responses to antigens in *M. tuberculosis*-infected cases (left) and healthy controls (right). The percentages of IFN-γ-producing CD4$^+$ T cells are shown. The long horizontal line represents the median, and the vertical line represents the interquartile range. The differences between control cells exposed to culture medium only (no antigen) and cells exposed to each antigen were assessed using the Wilcoxon matched-pairs signed rank test ($^{**}P < 0.01$, $^{*}P < 0.05$). (D) IL-2 responses to mHBHA in *M. tuberculosis*-infected cases, grouped according to the disease status as on-treatment TB cases ($n = 2$), recovery stage TB cases ($n = 5$), and contact cases ($n = 5$). Responses of control cases ($n = 8$) are also shown. The differences between each set of samples were assessed using the Mann-Whitney test ($^{*}P < 0.05$).

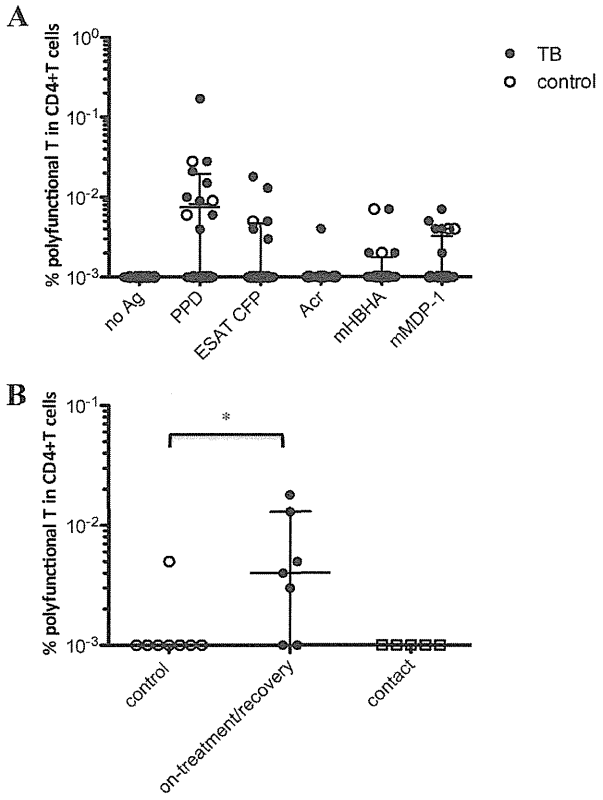

Fig. 3. Responses of polyfunctional CD4$^+$ T cells to *M. tuberculosis*-related antigens. (A) Percentages of polyfunctional (secreting both IFN-γ and IL-2) CD4$^+$ T cells following stimulation by various *M. tuberculosis*-related antigens. Filled circles represent the *M. tuberculosis*-infected cases, and open circles represent the healthy controls. (B) Percentages of polyfunctional CD4$^+$ T cells following stimulation by ESAT-6/CFP-10; *M. tuberculosis*-infected cases are grouped according to the disease status as either TB (on-treatment/recovery; $n = 7$) or contact cases ($n = 5$). Responses of control cases ($n = 8$) are also shown. The differences between control cells exposed to culture medium only and grouped *M. tuberculosis* cases were assessed using the Mann-Whitney test ($^*P < 0.05$). (A, B) The long horizontal line represents the median, and the vertical line represents the interquartile range.

tensity of T cells that produce multiple cytokines are highly correlated with protection in various infections and vaccination (26). In this study, polyfunctional CD4$^+$ T cells producing both IFN-γ and IL-2 were detected following all *M. tuberculosis*-related antigen stimulations. No polyfunctional CD4$^+$ T cells were detectable without antigen stimulation. Although the overall frequency of polyfunctional CD4$^+$ T cells following PPD stimulation was higher in the *M. tuberculosis*-infected cases than that in the healthy controls, three of the eight healthy controls showed a high frequency of polyfunctional CD4$^+$ T cells (Fig. 3A). The difference between the frequency of polyfunctional CD4$^+$ T cells in *M. tuberculosis*-infected cases and healthy controls was not significant for the other *M. tuberculosis*-related antigen stimulations (Fig. 3A); however, when the seven on-treatment and recovery stage *M. tuberculosis*-infected cases were analyzed separately from the five *M. tuberculosis* contact cases, the frequency of polyfunctional CD4$^+$ T cells following ESAT-6/CFP-10 stimulation was significantly higher in the on-treatment and recovery stage groups than that in the control group (Fig. 3B; $P = 0.0365$). These results suggest that the polyfunctional CD4$^+$ T cell response to this set of *M. tuberculosis*-specific antigens and not the IFN-γ response alone (Fig. 2B) has a diagnostic value for the detection of on-treatment and recovery stage TB cases.

IL-17A responses to some *M. tuberculosis*-related antigens are associated with active or latent *M. tuberculosis* infection: Compared with control cells exposed to culture medium, the percentage of CD4$^+$ T cells producing IL-17A was slightly but significantly increased by PPD and mHBHA stimulation ($P = 0.0117$ and 0.0233, respectively) (Fig. 4A). This increase was observed only in *M. tuberculosis*-infected cases and not in healthy controls (data not shown). Furthermore, when the on-treatment and recovery stage cases were analyzed separately from the contact cases, the IL-17A responses induced by mHBHA (Fig. 4B) and mMDP-1 (Fig. 4C) were significantly higher ($P = 0.0127$ and 0.0237, respectively) than those in healthy controls in the on-treatment and recovery stage groups only. Overall, these data suggest that an increased frequency of IL-17A-producing CD4$^+$ T cells is a supportive indicator of *M. tuberculosis* infection.

The frequency of IL-10-producing CD4$^+$ T cells is reduced following TB therapy: IL-13-producing CD4$^+$ T cells were not detected in the subjects included in this study. In *M. tuberculosis*-infected cases, the IL-10 responses to ESAT-6/CFP-10, mHBHA, and mMDP-1 were significantly higher than the response to culture medium alone ($P = 0.0413$, 0.0231, and 0.0144, respectively) (Fig. 5A). Notably, the frequency of Acr-stimulated IL-10-producing CD4$^+$ T cells in the recovery stage TB cases was significantly lower than that in the contact cases ($P = 0.0362$) (Fig. 5B). This trend needs to be confirmed with a larger cohort of TB cases.

DISCUSSION

In this study, we performed cross-sectional analysis of cytokine profiles in CD4$^+$ T cells from different clinical stages of TB infection, including on-treatment (active TB), recovery stage, and contact cases (both as non-active TB), following stimulation by PPD, ESAT-6/CFP-10, and other latency-associated *M. tuberculosis* antigens. We demonstrated here that the IFN-γ response alone was unable to distinguish between TB cases and healthy controls, even after exposure to a new set of latency-related *M. tuberculosis* antigens. However, when TB cases were grouped by distinct clinical stages of TB infection, significant differences between the recovery stage TB group and control group and between the recovery stage TB group and contact group were observed in the IL-2 response to mHBHA (Fig. 2D), and significant differences were observed between the recovery stage TB group and control group in the IL-17 response to mHBHA and mMDP-1 (Fig. 4B and 4C). Similarly, the number of *M. tuberculosis*-specific polyfunctional T cells producing both IFN-γ and IL-2 was also significantly different from that of the control group in ESAT-6/CFP-10 stimulation, which is consistent with previous findings (22). Thus, although further studies are necessary, our results indicate that cytokine

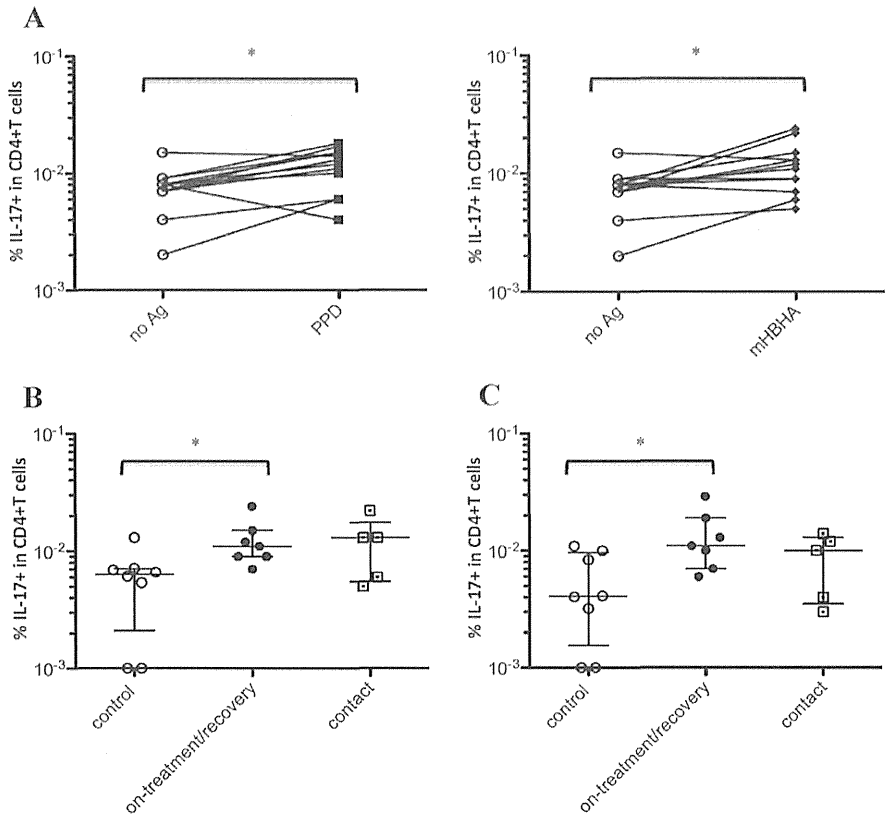

Fig. 4. IL-17 responses of CD4$^+$ T cells to *M. tuberculosis*-related antigens. (A) IL-17 responses to culture medium alone (no antigen), PPD, and mHBHA in *M. tuberculosis*-infected cases. The differences between control cells and each antigen were assessed using the Wilcoxon matched-pairs signed rank test ($^*P < 0.05$). (B, C) IL-17 responses to mHBHA (B) and mMDP-1 (C) in TB cases grouped according to the disease status as TB (on-treatment/recovery; $n = 7$) or contact cases ($n = 5$). Responses of control cases ($n = 8$) are also shown. The differences between control cells and each *M. tuberculosis* group were assessed using the Mann-Whitney test ($^*P < 0.05$). The long horizontal line represents the median and the vertical line represents the interquartile range.

profiles of various *M. tuberculosis*-related antigen-specific T cells can be useful parameters to assess TB status.

It is known that the clinical treatment of *M. tuberculosis* shifts the single IFN-γ-producing CD4$^+$ T cell response to both a polyfunctional IFN-γ/IL-2 response and a single IL-2 response (23). Therefore, while the dominant IFN-γ response is detectable during the active TB stage, dominant IL-2 responses are more likely to be detected at the non-active (contact and recovery) stage of the disease. Unfortunately, we were unable to address this issue in the present study because only two on-treatment cases were included; therefore, further studies with a larger sample size are warranted. Notably, the IL-2-producing CD4$^+$ T cell response was elevated in some patients prior to *M. tuberculosis* antigen stimulation. Because IL-2 is known to be crucial for the maintenance of Treg cells (24) and proliferation of Th cells (25), we speculated that these IL-2-producing CD4$^+$ T cells are on duty in vivo to regulate inflammatory responses caused by *M. tuberculosis* infection.

Polyfunctional *M. tuberculosis*-specific T cells have a memory function with proliferative capacity (19,26) as well as the ability to produce high quantities of cytokines (27). These functional abilities are necessary to control the propagation of foreign pathogens such as *M. tuberculosis*. Therefore, polyfunctional T cells are expected to be induced in *M. tuberculosis* cases with active bacterial replication, and some studies have reported that polyfunctional T cells are present at higher frequencies in active TB cases than those in healthy controls or latent TB cases (28,29). In the present study, significant levels of ESAT-6/CFP-10-specific polyfunctional CD4$^+$ T cells producing both IFN-γ and IL-2 were detected in TB cases only. An investigation of the TNF-α responses was not performed in this study owing to the color detection limitation of the flow cytometer employed. Recently, a large cohort investigation of ESAT-6- and CFP-10-induced polyfunctional *M. tuberculosis*-specific T cells (producing IFN-γ, IL-2, and TNF-α) in TB patients showed that the TNF-α-producing *M. tuberculosis*-specific CD4$^+$ T cell response is dominant and accurately reflects the active TB state (30). However, because frozen PBMC samples were used in the investigation, IFN-γ-producing CD4$^+$ T cells may have been exclusively lost, as observed in the present study (Fig. 1). Therefore, further studies are warranted to confirm this finding.

CD4$^+$ T cells that secrete IL-17 are considered as Th17 cells (17), which trigger early inflammatory via neutrophil recruitment (31). Because of the methylation at lysine residues, mycobacterial HBHA proteins are resistant to proteolytic degradation by proteases present in bronchoalveolar lavage fluids, and their abundance

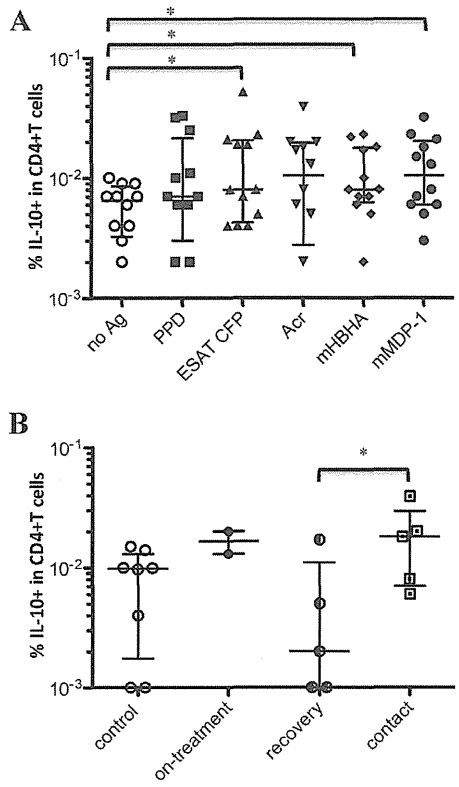

Fig. 5. IL-10 responses of CD4$^+$ T cells to *M. tuberculosis*-related antigens. (A) The percentages of IL-10 secreting CD4$^+$ T cells are shown. The differences between control cells and each antigen were assessed using the Wilcoxon matched-pairs signed rank test ($^*P < 0.05$). (B) IL-10 responses to Acr in *M. tuberculosis*-infected cases grouped according to the disease status as on-treatment TB cases ($n = 2$), recovery stage TB cases ($n = 5$), and contact cases ($n = 5$). Responses of control cases ($n = 8$) are also shown. The differences between each set of samples were assessed using the Mann-Whitney test ($^*P < 0.05$). (A, B) The long horizontal line represents the median and the vertical line represents the interquartile range.

in the cell membrane is believed to aid the attachment of *M. tuberculosis* to alveolar epithelial cells (32). Therefore, we postulated that HBHA proteins are one of the first antigens that the host immune system encounters and that the IL-17 response to HBHA proteins can be detected in a very early phase of *M. tuberculosis* infection or exposure. In the present study, we detected a small but significant number of IL-17A-producing CD4$^+$ T cells in response to HBHA in TB cases. This is compatible with a previous finding that HBHA-specific memory CD4$^+$ T cells are present in vivo (33). To clarify the role of this IL-17 immune response in the course of *M. tuberculosis* infection, it is worth investigating the IL-17 response to HBHA in a cohort of early *M. tuberculosis* exposure population.

The C-terminal domain of HBHA recognizes the lysine-rich domain to be the same as heparin-sulfate receptors, and MDP-1 has a heparin-binding site that resembles HBHA (34). We hypothesized that mMDP-1 could also induce an early host immune response in a similar manner to mHBHA. As expected, significant responses to mMDP-1 were detected in the on-treatment and recovery stage *M. tuberculosis* cases. Therefore, the Th17 response to HBHA and MDP-1 may be a candidate predictive marker of early *M. tuberculosis* infection.

IL-10 functions as an anti-inflammatory cytokine and has been suggested to contribute to the onset of infectious disease by inhibiting other inflammatory cytokines. IL-10 is also known to directly affect macrophages by inhibiting expression of MHC class II and costimulatory molecules (35). A high number of Treg cells, which are a known source of IL-10, are present in human TB granulomas (36). In this study, the IL-10 response was low in recovery stage TB cases and was even lower than that in contact TB cases (Fig. 5B). This result may be due to the migration of IL-10-producing T cells from the blood to local inflammatory sites. Alternatively, *M. tuberculosis*-specific IL-10-producing T cells may have a transient role during early infection and self-antigen-specific IL-10-producing T cells may contribute to halting inflammation (37). The candidate of self-antigen is a dump of *M. tuberculosis* granuloma. Thus, it is considered that the IL-10 response to *M. tuberculosis* antigen simply follows *M. tuberculosis* inflammation and that the IL-10 response may serve as a marker for resolving the disease.

The IL-2 response to mHBHA antigen in recovery stage TB cases was significantly higher than that in healthy controls and contact cases. This finding implies that the IL-2 response to mHBHA is a useful marker of LTBI. Recent analysis of the ratio of HBHA-induced and recombinant ESAT-6-induced IFN-γ responses suggested that latent TB patients can be categorized into three different risk groups (38). Here, we found that the ratio of mHBHA-induced and ESAT-6/CFP-10-induced IFN-γ T cell responses tended to decrease after longer post-treatment durations. Because HBHA molecules are enriched in the *M. tuberculosis* membrane, it is likely that the T cell responses to HBHA accurately reflect the TB burden. On the other hand, ESAT-6 is known to be important for suppressing host immunity by inhibiting macrophage function (39) and may be required when *M. tuberculosis* is present in granulomas. Therefore, the ratio of HBHA-induced to ESAT-6/CFP-10-induced T cell responses may vary at distinct clinical stages of TB.

In conclusion, this study employed various *M. tuberculosis*-related antigens, including a novel methylated MDP-1 antigen, to show that the cytokine profiles of CD4$^+$ T cells differ at each clinical stage of TB. The results indicate that the detection of *M. tuberculosis*-specific polyfunctional T cells reflects the onset of TB. A more accurate prediction of disease onset may be achieved by combining the detection of several cytokines such as IL-10 and IL-17, which are produced in response to various *M. tuberculosis*-related antigens. A combination of this approach with the detection of latent *M. tuberculosis*-related antigens may allow the development of an improved diagnostic test that can more accurately identify *M. tuberculosis*-infected individuals at a higher risk of developing TB and eventually form the basis of a public health measure for controlling *M. tuberculosis* infection. We believe that further analysis of a wide spectrum of T cell cytokine responses to latent *M. tuberculosis*-related antigens will help in the assessment of the disease status of TB patients and the initiation of an early therapeutic inter-

vention.

Acknowledgments We thank all participants that provided blood samples.

This work was supported by a grant from the Ministry of Health, Labour and Welfare of Japan.

Conflict of interest None to declare.

REFERENCES

1. Dye, C., Scheele, S., Dolin, P., et al. (1999): Consensus statement. Global burden of tuberculosis: estimated incidence, prevalence, and mortality by country. WHO Global Surveillance and Monitoring Project. JAMA, 282, 677–686.
2. Lawn, S.D. and Zumla, A.I. (2011): Tuberculosis. Lancet, 378, 57–72.
3. Horsburgh, C.R., Jr. (2004): Priorities for the treatment of latent tuberculosis infection in the United States. N. Engl. J. Med., 350, 2060–2067.
4. Tuberculosis Research Center, Chennai, India (2003): Association of initial tuberculin sensitivity, age and sex with the incidence of tuberculosis in South India: a 15-year follow up. Int. J. Tuberc. Lung Dis., 7, 1083–1091.
5. Pai, M., Riley, L.W. and Colford, J.M., Jr. (2004): Interferon-gamma assays in the immunodiagnosis of tuberculosis: a systematic review. Lancet Infect. Dis., 4, 761–776.
6. Diel, R., Loddenkemper, R. and Nienhaus, A. (2010): Evidence-based comparison of commercial interferon-gamma release assays for detecting active TB: a meta analysis. Chest, 137, 952–968.
7. Diel, R., Loddenkemper, R. and Nienhaus, A. (2012): Predictive value of interferon-gamma release assays and tuberculin skin testing for predicting progression from latent TB infection to disease state: a meta-analysis. Chest, 142, 63–75.
8. Yuan, Y., Crane, D.D. and Barry, C.E., 3rd. (1996): Stationary phase-associated protein expression in *Mycobacterium tuberculosis*: function of the mycobacterial alpha-crystallin homolog. J. Bacteriol., 178, 4484–4492.
9. Yuan, Y., Crane, D.D., Simpson, R.M., et al. (1998): The 16-kDa alpha-crystallin (Acr) protein of *Mycobacterium tuberculosis* is required for growth in macrophages. Proc. Natl. Acad. Sci. USA, 95, 9578–9583.
10. Menozzi, F.D., Rouse, J.H., Alavi, M., et al. (1996): Identification of a heparin-binding hemagglutinin present in mycobacteria. J. Exp. Med., 184, 993–1001.
11. Locht, C., Hougardy, J.M., Rouanet, C., et al. (2006): Heparin-binding hemagglutinin, from an extrapulmonary dissemination factor to a powerful diagnostic and protective antigen against tuberculosis. Tuberculosis, 86, 303–309.
12. Matsumoto, S., Yukitake, H., Furugen, M., et al. (1999): Identification of a novel DNA-binding protein from *Mycobacterium bovis* bacillus Calmette-Guerin. Microbiol. Immunol., 43, 1027–1036.
13. Matsumoto, S., Furugen, M., Yukitake, H., et al. (2000): The gene encoding mycobacterial DNA-binding protein I (MDPI) transformed rapidly growing bacteria to slowly growing bacteria. FEMS Microbiol. Lett., 182, 297–301.
14. Matsumoto, S., Matsumoto, M., Umemori, K., et al. (2005): DNA augments antigenicity of mycobacterial DNA-binding protein 1 and confers protection against *Mycobacterium tuberculosis* infection in mice. J. Immunol., 175, 441–449.
15. Lawn, S.D., Badri, M. and Wood, R. (2005): Tuberculosis among HIV-infected patients receiving HAART: long term incidence and risk factors in a South African cohort. AIDS, 19, 2109–2116.
16. Diedrich, C.R., Mattila, J.T., Klein, E., et al. (2010): Reactivation of latent tuberculosis in cynomolgus macaques infected with SIV is associated with early peripheral T cell depletion and not virus load. PloS One, 5, e9611.
17. Zhu, J. and Paul, W.E. (2008): CD4 T cells: fates, functions, and faults. Blood, 112, 1557–1569.
18. Seder, R.A., Darrah, P.A. and Roederer, M. (2008): T-cell quality in memory and protection: implications for vaccine design. Nat. Rev. Immunol., 8, 247–258.
19. Day, C.L., Mkhwanazi, N., Reddy, S., et al. (2008): Detection of polyfunctional *Mycobacterium tuberculosis*-specific T cells and association with viral load in HIV-1-infected persons. J. Infect. Dis., 197, 990–999.
20. Sutherland, J.S., Young, J.M., Peterson, K.L., et al. (2010): Polyfunctional CD4(+) and CD8(+) T cell responses to tuberculosis antigens in HIV-1-infected patients before and after antiretroviral treatment. J. Immunol., 184, 6537–6544.
21. Pethe, K., Bifani, P., Drobecq, H., et al. (2002): Mycobacterial heparin-binding hemagglutinin and laminin-binding protein share antigenic methyllysines that confer resistance to proteolysis. Proc. Natl. Acad. Sci. USA, 99, 10759–10764.
22. Sutherland, J.S., Adetifa, I.M., Hill, P.C., et al. (2009): Pattern and diversity of cytokine production differentiates between *Mycobacterium tuberculosis* infection and disease. Eur. J. Immunol., 39, 723–729.
23. Millington, K.A., Innes, J.A., Hackforth, S., et al. (2007): Dynamic relationship between IFN-gamma and IL-2 profile of *Mycobacterium tuberculosis*-specific T cells and antigen load. J. Immunol., 178, 5217–5226.
24. Chen, C.Y., Huang, D., Yao, S., et al. (2012): IL-2 simultaneously expands Foxp3+ T regulatory and T effector cells and confers resistance to severe tuberculosis (TB): implicative Treg-T effector cooperation in immunity to TB. J. Immunol., 188, 4278–4288.
25. Liao, W., Lin, J.X., Wang, L., et al. (2011): Modulation of cytokine receptors by IL-2 broadly regulates differentiation into helper T cell lineages. Nat. Immunol., 12, 551–559.
26. Day, C.L., Abrahams, D.A., Lerumo, L., et al. (2011): Functional capacity of *Mycobacterium tuberculosis*-specific T cell responses in humans is associated with mycobacterial load. J. Immunol., 187, 2222–2232.
27. Kannanganat, S., Ibegbu, C., Chennareddi, L., et al. (2007): Multiple-cytokine-producing antiviral CD4 T cells are functionally superior to single-cytokine-producing cells. J. Virol., 81, 8468–8476.
28. Young, J.M., Adetifa, I.M., Ota, M.O., et al. (2010): Expanded polyfunctional T cell response to mycobacterial antigens in TB disease and contraction post-treatment. PloS One, 5, e11237.
29. Caccamo, N., Guggino, G., Joosten, S.A., et al. (2010): Multifunctional CD4(+) T cells correlate with active *Mycobacterium tuberculosis* infection. Eur. J. Immunol., 40, 2211–2220.
30. Harari, A., Rozot, V., Enders, F.B., et al. (2011): Dominant TNF-alpha+ *Mycobacterium tuberculosis*-specific CD4+ T cell responses discriminate between latent infection and active disease. Nat. Med., 17, 372–376.
31. Laan, M., Cui, Z.H., Hoshino, H., et al. (1999): Neutrophil recruitment by human IL-17 via C-X-C chemokine release in the airways. J. Immunol., 162, 2347–2352.
32. Temmerman, S., Pethe, K., Parra, M., et al. (2004): Methylation-dependent T cell immunity to *Mycobacterium tuberculosis* heparin-binding hemagglutinin. Nat. Med., 10, 935–941.
33. Loxton, A.G., Black, G.F., Stanley, K., et al. (2012): Heparin-binding hemagglutinin induces IFN-γ+IL-2+IL-17+ Multifunctional CD4+T cells during latent but not active tuberculosis disease. Clin. Vaccine Immunol., 19, 746–751.
34. Aoki, K., Matsumoto, S., Hirayama, Y., et al. (2004): Extracellular mycobacterial DNA-binding protein 1 participates in mycobacterium-lung epithelial cell interaction through hyaluronic acid. J. Biol. Chem., 279, 39798–39806.
35. Moore, K.W., de Waal Malefyt, R., Coffman, R.L., et al. (2001): Interleukin-10 and the interleukin-10 receptor. Annu. Rev. Immunol., 19, 683–765.
36. Rahman, S., Gudetta, B., Fink, J., et al. (2009): Compartmentalization of immune responses in human tuberculosis: few CD8+ effector T cells but elevated levels of FoxP3+ regulatory T cells in the granulomatous lesions. Am. J. Pathol., 174, 2211–2224.
37. Ozeki, Y., Sugawara, I., Udagawa, T., et al. (2010): Transient role of CD4+CD25+ regulatory T cells in mycobacterial infection in mice. Int. Immunol., 22, 179–189.
38. Corbiere, V., Pottier, G., Bonkain, F., et al. (2012): Risk stratification of latent tuberculosis defined by combined interferon gamma release assays. PloS One, 7, e43285.
39. Welin, A., Eklund, D., Stendahl, O., et al. (2011): Human macrophages infected with a high burden of ESAT-6-expressing *M. tuberculosis* undergo caspase-1- and cathepsin B-independent necrosis. PloS One, 6, e20302.

frontiers in
MICROBIOLOGY

REVIEW ARTICLE
published: 09 July 2013
doi: 10.3389/fmicb.2013.00178

Development of human dendritic cells and their role in HIV infection: antiviral immunity versus HIV transmission

Yasuko Tsunetsugu-Yokota* and Mahmod Muhsen

Department of Immunology, National Institute of Infectious Diseases, Tokyo, Japan

Edited by:
Mei-Ru Chen, National Taiwan University, Taiwan

Reviewed by:
Ai Kawana-Tachikawa, University of Tokyo, Japan
Ryuta Sakuma, Tokyo Medical and Dental University, Japan

***Correspondence:**
Yasuko Tsunetsugu-Yokota, Department of Immunology, National Institute of Infectious Diseases, 1-23-1 Toyama, Shinjuku, Tokyo 162-8640, Japan
e-mail: yyokota@nih.go.jp

Although dendritic cells (DCs) represent a small cell population in the body, they have been recognized as professional antigen presenting cells and key players of both innate and acquired immunity. The recent expansion of basic knowledge concerning differentiation and function of various DC subsets will greatly help to understand the nature of protective immunity required in designing acquired immunodeficiency syndrome (AIDS) vaccines. However, human immunodeficiency virus (HIV) not only targets $CD4^+$ T cells but also myeloid cells, including macrophages and DC. When HIV infects DC, its replication is highly restricted in DC. Nevertheless, even a low level of HIV production is sufficient to enhance HIV replication in activated $CD4^+$ T cells, through antigen presentation activity by HIV-infected DC. Considering how antiviral immunity is initiated and memory response is maintained, such efficient DC–T cell transmission of HIV should play an important role in the disturbed immune responses associated with HIV infection. Recently, accessory proteins encoded by HIV have been shown to interact with various proteins in DC, and thereby affect DC–T cell transmission. In this review, we summarize the current understanding about DC biology, antiviral immune responses and DC restriction factors, all of which will be important issues for the development of an effective AIDS vaccine in the future.

Keywords: DC–T transmission, HIV, DC subsets, accessory proteins

INTRODUCTION

Since the discovery of dendritic cells (DCs) in the 1970s (Steinman, 2007), DC have long been recognized as: (1) professional antigen presenting cells expressing high levels of major histocompatibility complex (MHC) class II and other costimulatory molecules, (2) localizing to various tissues/organs, and (3) migrating to lymphoid tissues after antigen acquisition, to either initiate immune responses or induce tolerance by interaction with T cells (see review by Banchereau and Steinman, 1998).

In the 1990s, we (Tsunetsugu-Yokota et al., 1995) and several others demonstrated that DC are easily susceptible to human immunodeficiency virus type 1 (HIV-1) infection and can therefore also efficiently transmit virus to antigen-specific $CD4^+$ T cells, in spite of low levels of virus production. These earlier studies lead to further research into the role of DC in the pathogenesis of HIV infection, because DC–T cell interaction is considered to better reflect the physiological mode of cell-to-cell HIV-1 infection *in vivo* as compared to T-to-T or T-to-adherent cell interactions, which involve env-mediated membrane fusion (Sattentau, 2008). As our laboratory previously demonstrated, the close contact site between DC–T cells is consolidated by the presence of T cell receptor binding to MHC–antigen complex, followed by the interaction and mutual signaling of various costimulatory molecules (Tsunetsugu-Yokota et al., 1997).

A substantial number of reviews, focusing on HIV-1 transmission from DC to T cells (Rinaldo and Piazza, 2004; Wu and KewalRamani, 2006; Piguet and Steinman, 2007) have illustrated distinct features of cell-to-cell transmission. However, although the majority of studies focus on the close contact as a virological synapse (VS: a neuronal synapse like cell–cell contact structure for spreading virus infection), most of them do not consider the importance of antigen-dependent DC–T cell interaction, which is well-recognized as an Immunological synapse (IS: a synapse like cell–cell contact structure for activating immune response).

In this review, we will summarize the current understanding of various human DC subsets based on several outstanding recent findings in DC biology and of antiviral immune responses initiated by DCs, and discuss about newly identified DC restriction factors counteracting HIV-1 accessory proteins (e.g., Vif, Vpu, and Nef), which may have an impact on (1) the susceptibility of DC to HIV-1 infection and (2) the transmissibility of HIV from DC to T cells via VS or IS.

BIOLOGY OF DENDRITIC CELLS

DC originate from common myeloid precursor cells in the bone marrow, but are quite heterogeneous in terms of their localization, surface phenotype, and function. The major DC subsets are classical or conventional DC (cDC) and plasmacytoid DC (pDC). The development pathway and the lineage relationship of these DCs have been subjects of extensive investigation (see review by Steinman and Idoyaga, 2010). By analyzing bone marrow precursors *in vivo*, a current view of DC development and homeostasis has been established. In the bone marrow, monocytes and DC precursors (MDP) first develop into a common DC precursor (CDP) before continuing development into either a monocyte, or a cDC precursor (PreDC) and pDC, respectively (Fogg et al., 2006; Liu et al., 2009). PreDC, pDC, and monocytes subsequently migrate through blood to the spleen and lymph nodes, whereby preDC